Cellular/Molecular

Constitutive Phosphorylation as a Key Regulator of TRPM8 Channel Function

Bastián Rivera,[1,2*] Claudio Moreno,[1,2*] Boris Lavanderos,[1,2] Ji Yeon Hwang,[4] Jorge Fernández-Trillo,[5] Kang-Sik Park,[4] Patricio Orio,[6] Félix Viana,[5] Rodolfo Madrid,[1,2,3] and María Pertusa[1,2,3]

[1]Departamento de Biología, Facultad de Química y Biología, Universidad de Santiago de Chile, Santiago, 9160000, Chile, [2]Millennium Nucleus of Ion Channel-Associated Diseases, Santiago, 9160000, Chile, [3]Millennium Nucleus for the Study of Pain, Santiago, 9160000, Chile, [4]Department of Physiology, College of Medicine, Kyung Hee University, Seoul, 02447, Republic of Korea, [5]Instituto de Neurociencias, UMH-CSIC, San Juan de Alicante, 03550, Spain, and [6]Centro Interdisciplinario de Neurociencia de Valparaíso and Instituto de Neurociencia, Facultad de Ciencias, Universidad de Valparaíso, 2340000, Valparaíso, Chile

In mammals, environmental cold sensing conducted by peripheral cold thermoreceptor neurons mostly depends on TRPM8, an ion channel that has evolved to become the main molecular cold transducer. This TRP channel is activated by cold, cooling compounds, such as menthol, voltage, and rises in osmolality. TRPM8 function is regulated by kinase activity that phosphorylates the channel under resting conditions. However, which specific residues, how this post-translational modification modulates TRPM8 activity, and its influence on cold sensing are still poorly understood. By mass spectrometry, we identified four serine residues within the N-terminus (S26, S29, S541, and S542) constitutively phosphorylated in the mouse ortholog. TRPM8 function was examined by Ca^{2+} imaging and patch-clamp recordings, revealing that treatment with staurosporine, a kinase inhibitor, augmented its cold- and menthol-evoked responses. S29A mutation is sufficient to increase TRPM8 activity, suggesting that phosphorylation of this residue is a central molecular determinant of this negative regulation. Biophysical and total internal reflection fluorescence-based analysis revealed a dual mechanism in the potentiated responses of unphosphorylated TRPM8: a shift in the voltage activation curve toward more negative potentials and an increase in the number of active channels at the plasma membrane. Importantly, basal kinase activity negatively modulates TRPM8 function at cold thermoreceptors from male and female mice, an observation accounted for by mathematical modeling. Overall, our findings suggest that cold temperature detection could be rapidly and reversibly fine-tuned by controlling the TRPM8 basal phosphorylation state, a mechanism that acts as a dynamic molecular brake of this thermo-TRP channel function in primary sensory neurons.

Key words: corneal nerve endings; kinase activity; primary sensory neurons; staurosporine; thermotransduction; WS-12

Significance Statement

Post-translational modifications are one of the main molecular mechanisms involved in adjusting the sensitivity of sensory ion channels to changing environmental conditions. Here we show, for the first time, that constitutive phosphorylation of the well-conserved serine 29 within the N-terminal domain negatively modulates TRPM8 channel activity, reducing its activation by agonists and decreasing the number of active channels at the plasma membrane. Basal phosphorylation of TRPM8 acts as a key regulator of its function as the main cold-transduction channel, significantly contributing to the net response of primary sensory neurons to temperature reductions. This reversible and dynamic modulatory mechanism opens new opportunities to regulate TRPM8 function in pathologic conditions where this thermo-TRP channel plays a critical role.

Received Feb. 14, 2021; revised July 4, 2021; accepted Aug. 13, 2021.

*B.R. and C.M. contributed equally to this work.

Author contributions: B.R., C.M., B.L., J.Y.H., J.F.-T., K.-S.P., P.O., F.V., R.M., and M.P. performed research; B.R., C.M., B.L., J.Y.H., J.F.-T., K.-S.P., P.O., F.V., R.M., and M.P. analyzed data; B.R., C.M., B.L., J.F.-T., K.-S.P., P.O., F.V., R.M., and M.P. edited the paper; R.M. and M.P. designed research; M.P. wrote the first draft of the paper; M.P. wrote the paper.

This work was supported by Grants DICYT VRIDeI-USACH 022143PP to M.P. and R.M.; FONDECYT 1161733 to R.M. and M.P.; FONDECYT 1181076 to P.O.; Centro Basal AC3E FB0008 to P.O.; VRIDeI-USACH AP-539MM to R.M.; National Research Foundation of Korea NRF-2019R1A2C2003642 to K.-S.P.; MINECO PID2019-108194RB and the Severo Ochoa Program for Centers of Excellence in R&D SEV-2017-0723 to F.V.; the Millennium Nucleus of Ion Channel-Associated Diseases (MiNICAD) to R.M. and M.P.; and the Millennium Nucleus for the Study of Pain (MiNuSPain) to R.M. and M.P. R.M. also thanks VRIDeI-USACH for postdoctoral support to B.R. (02183MM). B.R. (21161660) and B.L. (21181611) thank Comisión Nacional de Investigación Científica y Tecnológica de Chile PhD fellowships. MiNICAD is a Millennium Nucleus supported by the Millennium Science Initiative of the Ministry of Science, Technology, Knowledge and Innovation (Chile). MiNuSPain is a Millennium Nucleus supported by the Millennium Science Initiative of the Ministry of Science, Technology, Knowledge and Innovation (Chile). The CINV is a Millennium Science Institute funded by Agencia Nacional de Investigación y Desarrollo de Chile Grant ICN09_022 of the Ministry of Science, Technology, Knowledge and Innovation (Chile). The funders had no role in study conception, design, data collection, and interpretation or in the decision to submit the manuscript for publication. We thank Richard Pino and Matías Campos for excellent technical assistance.

The authors declare no competing financial interests.

Correspondence should be addressed to María Pertusa at maria.pertusa@usach.cl.

https://doi.org/10.1523/JNEUROSCI.0345-21.2021

Introduction

Skin temperature reductions evoke a variety of sensations ranging from comfortable cooling to intense pain (Viana and Voets, 2019). Transduction of innocuous cold temperatures occurs at peripheral free nerve endings of cold thermoreceptor neurons (CTNs), that detect minimal temperature drops through their exquisitely thermosensitive machinery (McKemy, 2013, 2018; Almaraz et al., 2014; Madrid and Pertusa, 2014; Vriens et al., 2014; González et al., 2015). Suppression of their basal activity also plays a critical role in warm sensing (Paricio-Montesinos et al., 2020). In mammalian CTNs, the key molecular cold sensor is TRPM8, a Ca^{2+}-permeable nonselective cation channel, activated by cold temperatures and cooling compounds, such as menthol (McKemy et al., 2002; Peier et al., 2002), voltage (Brauchi et al., 2004; Voets et al., 2004), and discrete rises in osmolality (Quallo et al., 2015). This thermo-TRP channel is not only involved in physiological temperature sensing but also plays critical roles in neuropathic and inflammatory pain and different types of cancer (McCoy et al., 2011; Pérez de Vega et al., 2016). Modulation of TRPM8 function entails several forms of molecular regulation, including membrane phosphoinositides (Liu and Qin, 2005; Rohacs et al., 2005; Yudin et al., 2011), interacting proteins (Zhang et al., 2012; Tang et al., 2013; Gkika et al., 2015), TRPM8 splice variants (Sabnis et al., 2008; Bidaux et al., 2016), and post-translational modifications (PTMs) (Pertusa and Madrid, 2015). Among these PTMs, N-glycosylation at the asparagine 934 in the pore loop of TRPM8 (Dragoni et al., 2006; Erler et al., 2006) mediates the association of the channel to lipid rafts (Morenilla-Palao et al., 2009), modulates channel gating, and sets the temperature threshold of CTNs (Pertusa et al., 2012), contributing to the marked differences in cold sensitivity observed between recombinant and native TRPM8 channels (de la Peña et al., 2005; Mälkiä et al., 2007; Pertusa et al., 2012).

Previous studies found that TRPM8 is regulated by different phosphorylation cascades. In sensory neurons and recombinant systems, protein kinase C (PKC) activation produces functional downregulation of TRPM8 (Premkumar et al., 2005; Abe et al., 2006; Linte et al., 2007; Sarria and Gu, 2010; Pabbidi and Premkumar, 2017; Rivera et al., 2020). The involvement of protein kinase A (PKA) in TRPM8 regulation is more controversial. Some studies described that forskolin or 8-Br-cAMP, activators of the adenylate cyclase (AC)/cAMP/PKA pathway, reduce TRPM8 activity (De Petrocellis et al., 2007; Linte et al., 2007). In contrast, a different study reported that AC inhibition decreases responses to agonists, suggesting that basal PKA activity upregulates TRPM8 function (Bavencoffe et al., 2010). This observation could imply that TRPM8 phosphorylation occurs under resting conditions; that is, when kinase activity is not stimulated over a basal level, and the proteome's phosphorylation state is maintained by a tonic balance in kinase/phosphatase activity. In that regard, a recent study reported that the *src* kinase constitutively phosphorylates TRPM8 at tyrosine residues (Manolache et al., 2020). There is also evidence that TRPM8 has a basal level of serine phosphorylation (Premkumar et al., 2005). Nevertheless, the specific TRPM8 residues that are constitutively phosphorylated are unknown, and the effect of this PTM on channel function and the molecular mechanism behind this modulation are still undefined.

Differences in protein phosphorylation pattern appear to be tissue-specific (Huttlin et al., 2010). Moreover, changes in phosphorylation status can also be observed under different pathologic conditions, including cancer (Ardito et al., 2017). Because TRPM8 expression is not restricted to somatosensory neurons (Almaraz et al., 2014), and this channel is involved in several pathologies, analyzing the role of basal phosphorylation in TRPM8 regulation in specific cellular contexts is of broad relevance. Here, we examined the contribution of constitutive phosphorylation to TRPM8 function. We show that basal phosphorylation alters the biophysical properties and trafficking of this polymodal thermo-TRP channel, identified the phosphorylated residues involved in this modulation and explored its influence on the thermosensitivity of primary sensory neurons expressing TRPM8.

Materials and Methods

Molecular biology and site-directed mutagenesis. Mouse TRPM8-myc and mouse TRPM8-YFP channels have been described previously (Pertusa et al., 2014). Single point mutants were obtained by overlap extension PCR, using Pfu ultra polymerase (Agilent Technologies). Before use, all plasmids were verified by DNA sequencing (Macrogen Korea).

Animals. This study was performed using male and female young adult (P21-P40) C57BL/6 mice. Animals were housed at a maximum of 4 per cage in a 12 h light/dark cycle with food and water *ad libitum*, and killed with CO_2. All experiments were conducted according to the bioethical guidelines of the Agencia Nacional de Investigación y Desarrollo de Chile (former Comisión Nacional de Investigación Científica y Tecnológica de Chile) and have been approved by the Bioethical Committee of the Universidad de Santiago de Chile (reference number 289/2018).

Cell culture. Trigeminal ganglia (TG) were extracted and incubated in an enzymatic mixture in INC-mix solution (in mM as follows: 155 NaCl, 1.5 K_2HPO_4, 10 HEPES, 5 glucose, pH 7.4) containing dispase (5 IU/ml; 17105-041 Invitrogen-Thermo Fisher Scientific) and collagenase Type XI (650 IU/ml; C7657, Sigma-Aldrich) for 40 min at 37°C in 5% CO_2. The TG were then mechanically dissociated with polished Pasteur pipettes, and the neurons were plated on poly-L-lysine-coated 6 mm #0 glass coverslips (Menzel-Gläser), maintained in MEM (Earle's salts, 11095080, Invitrogen-Thermo Fisher Scientific) supplemented with MEM-vit (11120052, Invitrogen-Thermo Fisher Scientific), 10% FBS (SH30910.03, Hyclone, General Electric Healthcare Life Science), 200 µg/ml streptomycin, 125 µg/ml penicillin (15140-122, Invitrogen-Thermo Fisher Scientific), and used within 6-12 h for patch-clamp recordings and Ca^{2+} imaging.

Heterologous expression of TRPM8. HEK293, F11, or COS-7 cells were plated onto 24-well plates at 1×10^5 cells/well, and transiently transfected with 1 µg of indicated DNA and Lipofectamine 2000 (Invitrogen-Thermo Fisher Scientific), following the manufacturer's indications. At 48 h after transfection, Ca^{2+} imaging, patch-clamp, and total internal reflection fluorescence (TIRF) experiments were performed. A HEK293 cell line stably expressing TRPM8 (HEK293-mTRPM8-myc cells) was used in this study (Cornejo et al., 2020). Cell lines were cultured in DMEM containing 10% FBS and antibiotics (100 µg/ml streptomycin/penicillin for HEK293 and COS-7 cells and 600 µg/ml geneticin [Corning Life Sciences] for HEK293-mTRPM8-myc cell line). Twenty-four hours before experimental procedures, cells were trypsinized and plated on poly-L-lysine-coated 6 mm #0 glass coverslips (Menzel-Gläser) for Ca^{2+} imaging and patch-clamp experiments and 24 mm #1 glass coverslips (Menzel-Gläser) for TIRF microscopy.

Immunoprecipitation and Western blot. Cell extracts from HEK293-mTRPM8-myc were lysed in standard lysis buffer containing 1% v/v Triton X-100, 150 mM NaCl, 1 mM EDTA, 50 mM Tris-HCl, pH 7.4, supplemented with 1/100 Halt Protease & Phosphatase Inhibitor Cocktail (Invitrogen-Thermo Fisher Scientific). Lysates were subjected to immunoprecipitation with commercial antibodies against the c-Myc epitope (Sigma-Aldrich). Immunocomplexes were incubated for 6 h at 4°C with protein G-Sepharose (Roche Applied Science). After one wash with 1 ml of lysis buffer, immunoprecipitates were treated with 300 µl of FastAP (FastAP Thermosensitive Alkaline Phosphatase) reaction buffer phosphatase, with or without 20 U of FastAP (Thermo Fisher Scientific) for 2 h at room temperature. Finally, immunocomplexes were washed one

more time in lysis buffer. The whole extract and the immunoprecipitates were loaded onto a 7.5% SDS-PAGE. Proteins were transferred to a nitrocellulose membrane, blocked with 10% skim milk or 5% BSA in PBS, and incubated with antibodies against the Myc epitope (Santa Cruz Biotechnology) and GAPDH (Sigma-Aldrich), diluted to 1:4000 and 1:15,000, respectively, in T-PBS, and anti-phosphoserine (Sigma-Aldrich) and anti-phosphothreonine (Abcam) diluted to 1:3000 and 1:6000, respectively. HRP-coupled secondary antibodies (Sigma-Aldrich) were used at a final concentration of 1:2000 for detection, and the signal was visualized using a Super Signal West Dura Chemiluminescent kit (Invitrogen-Thermo Fisher Scientific).

In-gel digestion and mass spectrometry (MS) analysis. TRPM8 bands (~130 kDa) from HEK293-mTRPM8-myc lysates subjected to immunoprecipitation were directly excised. In-gel digestion was performed in 50 ng/ml trypsin as described by Cerda et al. (2015). A nanoACQUITY UltraPerformance LC System (Waters) directly coupled with an LTQ Orbitrap Elite mass spectrometer (Thermo Fisher Scientific) equipped with a nano-electrospray source was used. Tryptic peptide mixtures were desalted and concentrated on the reverse phase trap column for 10 min at a flow rate of 5 µl/min, and trapped peptides were back-flushed onto a homemade microcapillary column (i.d. 100 µm, length 200 mm, 3 µm C_{18} particle size) for separation. Mobile Phases A and B were composed of 0% and 100% acetonitrile, respectively, and each contained 0.1% FA. The elution gradient was as follows: 5% B between 0 and 15 min, 0%-15% B over 5 min, 15%-50% B over 75 min, and 75%-95% B over 1 min. B was maintained at 95% for 13 min and then decreased to 5% B for 1 min. The column was finally re-equilibrated with 5% B for 10 min. During the chromatographic separation, the LTQ Orbitrap Elite was operated in a data-dependent mode. Mascot searches for LCMS/MS data were performed for the MS/MS dataset against the mouse Swiss-Prot database with phosphorylation on Ser, Thr, and Tyr and oxidation on Met. Every MS/MS spectrum that exhibited possible phosphorylation was manually checked and validated based on the existence of a 98 Da mass loss (H_3PO_4: phosphopeptide-specific CID neutral loss) for both the precursor and the fragmented ions.

Ca^{2+} imaging. Ratiometric Ca^{2+} imaging experiments were conducted using the fluorescent indicator fura-2 AM (F1221, Thermo Fisher Scientific). Before each experiment, cells were incubated with 5 µM fura-2 AM in standard extracellular solution supplemented with 0.02% pluronic acid (P6867, Invitrogen-Thermo Fisher Scientific), for 50 min at 37°C in darkness. The standard extracellular solution, referred to as the control solution, contained the following (in mM): NaCl 140, KCl 3, $CaCl_2$ 2.4, $MgCl_2$ 1.3, HEPES 10, glucose 10, and was adjusted to pH 7.4 with NaOH. Fluorescence measurements were obtained using an inverted Nikon Ti microscope equipped with a Super Plan Fluor ELWD 20XC objective N.A. 0.45 (Nikon Instruments) and a 12-bit cooled ORCA C8484-03G02 CCD camera (Hamamatsu). Fura-2 was excited at 340 and 380 nm with a Polychrome V monochromator (Till Photonics, Thermo Fisher Scientific), with exposure times no longer than 40 ms; the emitted fluorescence was filtered with a 510 nm long-pass filter. Fluorescence ratios (0.5 Hz) were displayed online with HCImage version 2 software (Hamamatsu).

Bath temperature (see details below) was sampled simultaneously using a BAT-12 microprobe thermometer (Physitemp Instruments) supplemented with an IT-18 T-thermocouple, using Clampex 10 software (Molecular Devices). The signal was digitized with an Axon Digidata 1440A AD converter (Molecular Devices).

Threshold temperature values for the rise in $[Ca^{2+}]_i$ were estimated as in González et al. (2017). The temperature was linearly interpolated at the midpoint between the baseline and the first point at which $[Ca^{2+}]_i$ elevation deviates by at least 4 times the SD of the baseline.

TIRF microscopy. Cells on 24 mm glass round coverslips were placed in a custom-made chamber, and imaging experiments were performed at ~30°C, using extracellular control solution. TIRF images were acquired using a TIRF system built around an inverted Nikon TE2000-U microscope equipped with a 60×/1.49 oil immersion ApoTIRF objective, an Andor iXon+ 888 CCD camera (Oxford Instruments), and a 491 nm laser (Calypso 100, Cobolt). Laser light was filtered and power regulated using an acoustic optical tunable filter (Till Photonics-AOTF, Thermo Fisher Scientific). The microscope filter cube contained a Dual 488/561 HC BrightLine laser filter set (Semrock). Time series of images at 10 s intervals were recorded, with an exposure time of 200 ms. Image acquisition and fluorescence intensity analysis were performed using Live Acquisition processing software (Till Photonics, Thermo Fisher Scientific).

Electrophysiology. Whole-cell patch-clamp recordings in transfected HEK293 cells were performed simultaneously with temperature recordings. Standard patch pipettes (3-5 MΩ) were made of GC150F-7.5 borosilicate glass capillaries (Harvard Apparatus) and contained the following (in mM): 130 CsCl, 1 EGTA, 10 HEPES, 4 ATP-Mg, and 0.4 GTP-Na, pH adjusted to 7.4 with CsOH. The bath solution was the same as in the Ca^{2+} imaging experiments. Current signals were recorded with an Axopatch 200B patch-clamp amplifier (Molecular Devices). Stimulus delivery and data acquisition were performed using pClamp10 software (Molecular Devices). Current-voltage (*I–V*) relationships obtained from repetitive (0.2 Hz) voltage ramps (−100 to 180 mV, with a slope of 200 mV/s) were fitted with a function that combines a linear conductance multiplied by a Boltzmann activation term (Nilius et al., 2006) to estimate the shifts in the voltage-dependent TRPM8 activation as follows:

$$I = g \times (V - E_{rev}) / \left(1 + exp[(V_{1/2} - V)/s]\right) \quad (1)$$

where g is the whole-cell conductance, E_{rev} is the reversal potential of the current, $V_{1/2}$ is the potential for half-maximal activation, and s is the slope factor. Examples of these fittings are shown in Figure 3*C*.

For whole-cell recordings of cold-evoked currents in trigeminal neurons, standard patch pipettes (4-5 MΩ resistance) were made using GC150F-7.5 borosilicate glass capillaries (Harvard Apparatus) and filled with intracellular solution containing the following (in mM): CsCl 140, $MgCl_2$ 0.6, EGTA 1, HEPES 10, ATP-Na_2 1, and GTP-Na 0.1 (pH 7.4 adjusted with CsOH). Before patch-clamp recordings in CTNs, the temperature threshold in response to cold stimuli was determined using Ca^{2+} imaging in control solution. The bath solution used to measure the activation of I_{TRPM8} in cold thermoreceptors contained the following (mM): NaCl 140, KCl 3, $MgCl_2$ 1.3, $CaCl_2$ 0.1, HEPES 10, glucose 10 (pH 7.4 adjusted with NaOH), and was supplemented with 0.5 µM TTX.

Temperature stimulation. Coverslips with cultured cells were placed in a microchamber and continuously perfused with solutions warmed to ~35°C. The temperature was adjusted with a water-cooled Peltier device that was computer-controlled and placed at the inlet of the recording chamber, controlled by a feedback device. Cold sensitivity was evaluated with temperature drops from ~35°C to 19°C.

Variance analysis. To estimate the number of active TRPM8 channels at the plasma membrane, we used nonstationary noise analysis (Alvarez et al., 2002). One hundred current records in whole-cell configuration were collected for each cell, during activation of the channels by 150 ms depolarizing voltage steps from 0 to 180 mV, at 19°C (Pertusa et al., 2012, 2018; Rivera et al., 2020). Ensemble averaged current ($<I>$) and its variance (σ^2) on each isochrone were calculated. The variance as a function of $<I>$ was fitted using the following equation:

$$\sigma^2 = i * <I> - (<I>^2/N) \quad (2)$$

where i is the single-channel unitary current and N is the number of channels in the plasma membrane. The maximum open probability (Po_{max}) was estimated using the relation $Po_{max} = I_{max}/i*N$, where I_{max} is the mean maximal current in each experiment. Data for variance analysis were acquired at 20 kHz and filtered at 5 kHz.

Mathematical model. To explore the correlation between firing frequency and TRPM8 functional expression level, we used the model of cold-sensitive neurons (CSNs) that includes TRPM8, first described by Olivares and colleagues (Olivares and Orio, 2015; Olivares et al., 2015). The equation for the membrane potential is as follows:

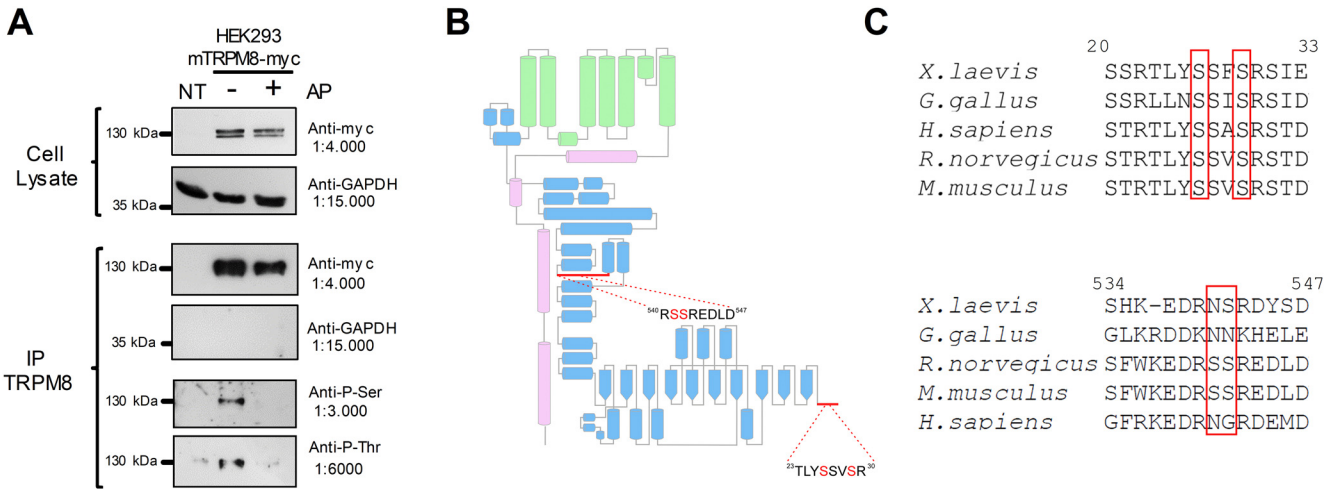

Figure 1. The TRPM8 channel is a phosphoprotein in basal conditions. ***A***, Immunopurification (IP) of TRPM8 with anti-myc antibody from nontransfected HEK293 cells (NT) and HEK293-mTRPM8-myc cells extracts, untreated or treated with alkaline phosphatase (AP). Western blot of cell extracts and IPs showing the bands corresponding to TRPM8-myc and GAPDH. Phosphorylation of Ser and Thr residues were determined using phosphoserine (Anti-P-Ser) and phosphothreonine (Anti-P-Thr) antibodies. ***B***, Scheme of a TRPM8 subunit showing its secondary structure elements described by Yin et al. (2018). Green represents transmembrane domains. Blue represents N-terminal domain. Magenta represents C-terminus. Modified from Pertusa et al. (2018). Close-up view of the proximal and distal N-terminal domain, showing the detail of the sequence where phosphorylated residues were identified using MS. ***C***, Alignment of distal and proximal N-terminal domains of *Xenopus laevis*, *Gallus gallus*, *Rattus norvegicus*, *Mus musculus*, and *Homo sapiens* TRPM8 orthologs using ClustalW (Sievers et al., 2011) and Jalview (Waterhouse et al., 2009). Numbers correspond to residues in mTRPM8. Red boxes highlight the conservation of phosphorylation sites.

$$C_m = \frac{dV}{dt} = -I_{Sd} - I_{ST} - I_d - I_r - I_{M8} - I_l + I_{wn} \quad (3)$$

where C_m is the membrane capacitance, I_{sd} and I_{sr} are, respectively, the slow depolarizing and repolarizing currents that create the intrinsic oscillation of membrane potential. I_d and I_r are Hodgkin and Huxley-type depolarizing and repolarizing currents for action potential firing, I_{M8} is the TRPM8-dependent cold-activated current, I_l is an ohmic leakage current, and I_{wn} is a noise term. Ionic currents are given by the following:

$$I_i = g_i a_i (V - E_i) \quad (i = sd, sr, d, r, M8, l) \quad (4)$$

where *gi* represents the maximum conductance density of the current *i*, given by the channel expression level. E_i is the reversal potential of the current, and a_i is the activation variable or open channel probability, usually voltage-dependent except for $a_l \equiv 1$ (for the rest of the equations and details, see Olivares and Orio, 2015; Olivares et al., 2015). The brake I_{KD} current is contained in the rest of the parameters considered in the model; therefore, it is invariant in all simulations.

As in our previous studies (Olivares et al., 2015; Piña et al., 2019), we used different sets of parameters that result in different types of dynamic responses. In addition, we generated sets of parameters that resemble the behavior of cultured CSNs, with no spontaneous activity at basal temperature (33°C-35°C) and a strong spiking response starting at variable thresholds between 33.5°C and 18.5°C. The parameters sets used in this study are listed in Extended Data Fig. 11-1 (for CSNs) and Extended Data Fig. 12-1 (for cold-sensitive nerve endings; these individuals were used in Rivera et al., 2020), and they all share the following common parameters:

C_m= 1 (μF/cm^2); E_l= −70, E_d= E_{sd}= 50, E_r= E_{sr}= −90, E_{M8}= 0 (mV);

τ_{sd}= 10, τ_{sr}= 24, τ_r= 1.5 (ms); s_{sd}= 0.1, s_d= s_r= 0.25 (mV^{-1}); V^h_{sd}= −40, V^h_d= V^h_r= −25 (mV);

η = 0.012 (cm^2/μA); κ = 0.17; z_{M8}= 0.65 (mV^{-1}); ΔE= 9000 (J);

$K_{Ca,M8}$= 0.5 (μM); *d*= 1 (μm); *D*= 0.5 (μA/cm^2); τ_{wn} = 1 (ms).

The model was implemented in the Neuron simulation environment (RRID:SCR_005393), controlled with Python scripts (RRID:SCR_008394) (Hines and Carnevale, 1997; Hines, 2009). Analysis of the simulations was performed in Python with the libraries Numpy (RRID:SCR_008633), Scipy (RRID:SCR_008058), and Matplotlib (RRID:SCR_008624).

Data analysis. Data are reported as the mean ± SEM or mean ± SD from *n* cells studied. Unless mentioned otherwise, when comparing two mean values, statistical significance ($p < 0.05$) was assessed using Student's unpaired, two-tailed *t* test. For unpaired *t* test, Welch's correction was applied in the case of unequal variances. For multiple comparisons of means, one-way ANOVA was performed in combination with a Bonferroni's or Dunnett's *post hoc* test. Fisher's (*F*) exact test was used for the analysis of contingency tables. Data analysis was performed using PRISM 5 (GraphPad Software). All exact *p* values, statistical tests, and sample sizes are reported in the main text or figure legends.

Reagents and drugs. L-Menthol (266523), phorbol 12-myristate 13-acetate (PMA, P8139), and staurosporine solution in DMSO (S6942) were purchased from Sigma-Aldrich. (1R,2S,5R)-N-(4-methoxyphenyl)-5-methyl-2-propan-2-ylcyclohexane-1-carboxamide (WS-12, 3040) and TTX (1078) were purchased from Tocris Bioscience.

Table 1. Phosphorylated positions in the TRPM8 channel obtained by MS analysis[a]

	Peptide sequence	Score	Rank	Phosphosite
Control				
	^{23}TLY**pS**SVSR^{30}	28	1	Ser^{26}
	^{23}TLYSSV**pS**R^{30}	40	1	Ser^{29}
	^{538}EDRS**pS**REDLDVELHDASLTTR^{558}	81	1	Ser^{542}
	^{538}EDR**pS**SREDLDVELHDASLTTR^{558}	15	1	Ser^{541}
1 μM PMA				
	^{23}TLY**pS**SVSR^{30}	37	1	Ser^{26}
	^{23}TLYSSV**pS**R^{30}	31	1	Ser^{29}
	^{31}STDV**pS**YSDSDLVNFIQANFK^{50}	101	1	Ser^{35}
	^{538}EDRS**pS**REDLDVELHDASLTTR^{558}	16	1	Ser^{542}
	^{541} *p(SS)*REDLDVELHDASLTTR^{558}	38	1	Ser^{541}, Ser^{542}

[a]MS analysis (see Materials and Methods) was performed under control conditions and after a 10 min incubation with 1 μM PMA. Boldface type indicates unambiguous phosphorylation site. Italics indicates that the peptide has a phosphorylation but which residue was phosphorylated was not determined.

Results

TRPM8 is a constitutive serine-phosphorylated protein

Our first goal was to assess TRPM8 phosphorylation state under resting conditions. For this, we purified protein extracts from a stable cell line expressing a myc-tagged mouse TRPM8 (HEK293-mTRPM8-myc cells) using anti-myc antibodies. In agreement with

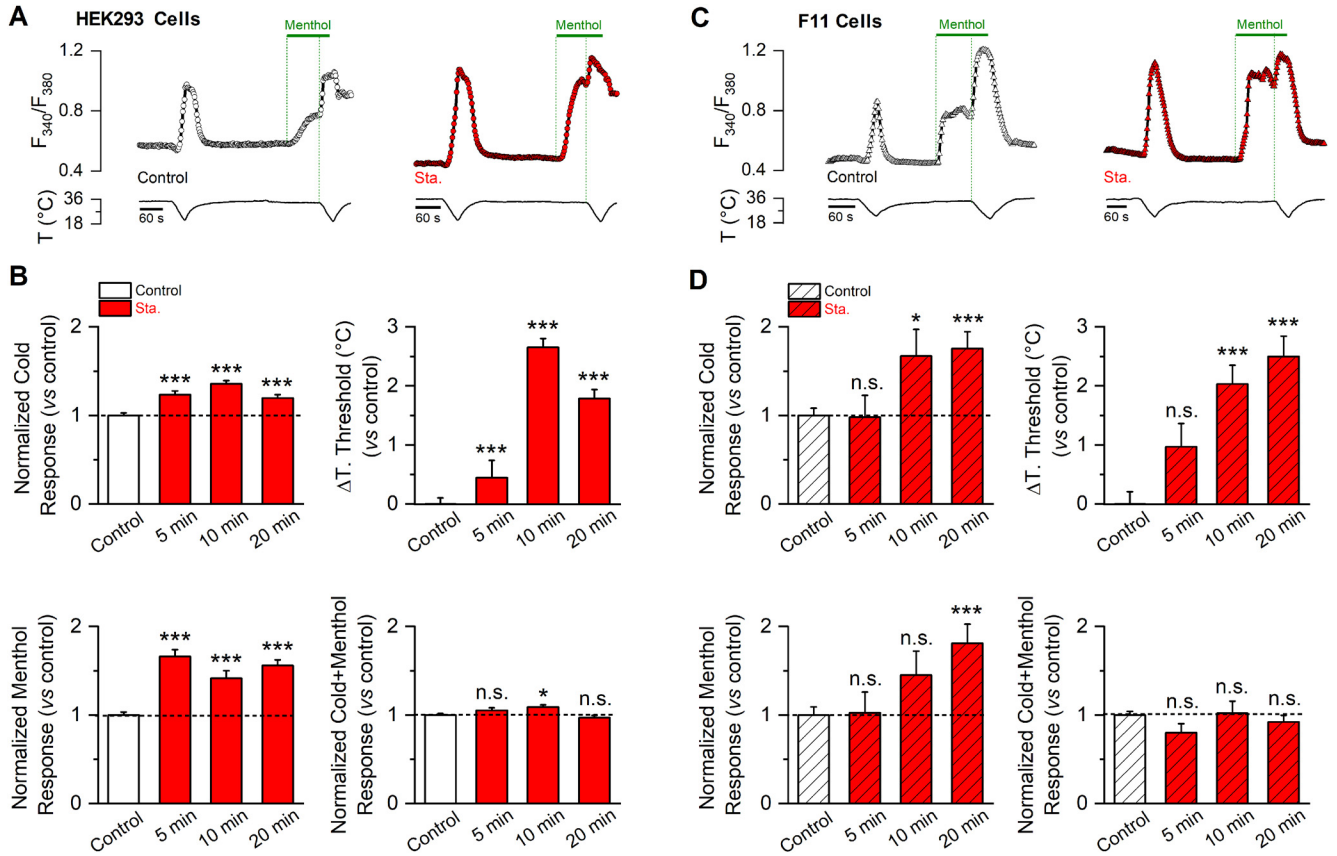

Figure 2. Basal kinase activity downregulates TRPM8 channel function. ***A***, Time course of $[Ca^{2+}]_i$ (F_{340}/F_{380}) responses to cold, 100 μM menthol, and to a combined stimulus of cold in the presence of 100 μM menthol of HEK293-mTRPM8-myc cells, in control conditions (open circles) and after a 10 min preincubation with staurosporine 200 nM (red circles). ***B***, Mean and SEM amplitude of cold-, menthol-, and Cold+menthol-induced responses in HEK293-mTRPM8-myc cells in control conditions and after 5, 10, and 20 min preincubation with 200 nM staurosporine (Sta.). The values were normalized to the mean response observed in control conditions in parallel experiments (Ctrl., $n = 230$; 5 min Sta., $n = 95$; 10 min Sta., $n = 89$; 20 min Sta., $n = 92$). Mean shift in temperature threshold (ΔT. threshold) displayed by staurosporine treatment is expressed according to the control values. Positive values indicate shifts toward warmer temperatures. Statistical analysis was performed using one-way ANOVA test (cold: $F_{(3,502)} = 21.00$, $p < 0.0001$, ΔT°. threshold: $F_{(3,502)} = 62.67$, $p < 0.0001$; menthol: $F_{(3,502)} = 48.63$, $p < 0.0001$; Cold+menthol: $F_{(3,502)} = 4.69$, $p = 0.0031$) in Dunnett's *post hoc* test: $^*p < 0.05$; $^{**}p < 0.01$; $^{***}p < 0.001$; ns, $p > 0.05$, compared with the control. ***C***, Time course of $[Ca^{2+}]_i$ (F_{340}/F_{380}) responses in F11 cells expressing mTRPM8-YFP channels, using the same protocol as in ***A***. ***D***, Mean and SEM amplitude of cold-, menthol-, and Cold+menthol-induced responses of TRPM8 in control conditions and after 5, 10, and 20 min preincubation with staurosporine 200 nM (Sta.). The values were normalized to the mean response observed in control conditions in parallel experiments (Control, $n = 88$; 5 min Sta., $n = 24$; 10 min Sta., $n = 24$; 20 min Sta., $n = 35$). Mean shift in temperature threshold displayed by staurosporine treatment is expressed according to the control values. Positive values indicate shifts toward warmer temperatures. Statistical analysis was performed using the one-way ANOVA test (cold: $F_{(3,167)} = 6.46$, $p = 0.0004$, ΔT. threshold: $F_{(3,167)} = 17.30$, $p < 0.0001$; menthol: $F_{(3,167)} = 5.47$, $p = 0.0013$; Cold+menthol: $F_{(3,167)} = 1.32$, $p = 0.2689$) in combination with a Dunnett's *post hoc* test: ns, $p > 0.05$; $^*p < 0.05$; $^{**}p < 0.01$; $^{***}p < 0.001$, compared with the control.

a previous report (Premkumar et al., 2005), Western blot analysis with anti-phosphoserine and anti-phosphothreonine antibodies showed a band corresponding to TRPM8 from the immunoprecipitation extracts, indicating that basal phosphorylation occurs in both serine and threonine residues. Importantly, this signal was not present in immunoprecipitation extracts from nontransfected HEK293 cells and was strongly attenuated when the protein extracts were treated with alkaline phosphatase, validating the specificity of this band (Fig. 1*A*).

Our next step was to identify the TRPM8 residues where this PTM occurs using MS analysis. To optimize the detection of phosphorylation sites, we used purified recombinant mTRPM8 protein extracted from the myc-tagged TRPM8 cell line. Proteins were size-fractionated by SDS-PAGE, and the corresponding TRPM8 bands were separated and analyzed using MS. TRPM8 peptides were identified using a Mascot database search, resulting in a 57% overall coverage of the whole TRPM8 protein sequence and 72% coverage of the cytoplasmic regions. Using this strategy, we identified serines 26 and 29 in the distal part of the N-terminus, and serines 541 and 542 located in the more proximal region of this domain (Table 1), as unambiguously phosphorylated residues in resting conditions (Fig. 1*B*). Comparison across species revealed that S26 and S29 are present in several TRPM8 orthologs, whereas S541 and S542 are not conserved (Fig. 1*C*). Since PKC can alter the TRPM8 phosphorylation pattern (Premkumar et al., 2005), we also analyzed samples from cells treated with 1 μM PMA, a chemical activator of this kinase. Interestingly, phosphorylation of S26, S29, S541, and S542 was again detected in this analysis (Table 1), along with an additional phosphorylation site at S35, which could result from PKC-dependent pathway activation.

Basal phosphorylation downregulates TRPM8 function

To evaluate the relevance of constitutive phosphorylation on TRPM8 function, we reduced basal kinase tone with staurosporine, a broad kinase inhibitor. Taking advantage that TRPM8 is a Ca^{2+}-permeable channel, we first characterized the responses of TRPM8 channels to agonists in a recombinant system using Ca^{2+} imaging, a well-established noninvasive approach to study this channel that avoids potential disruption of relevant

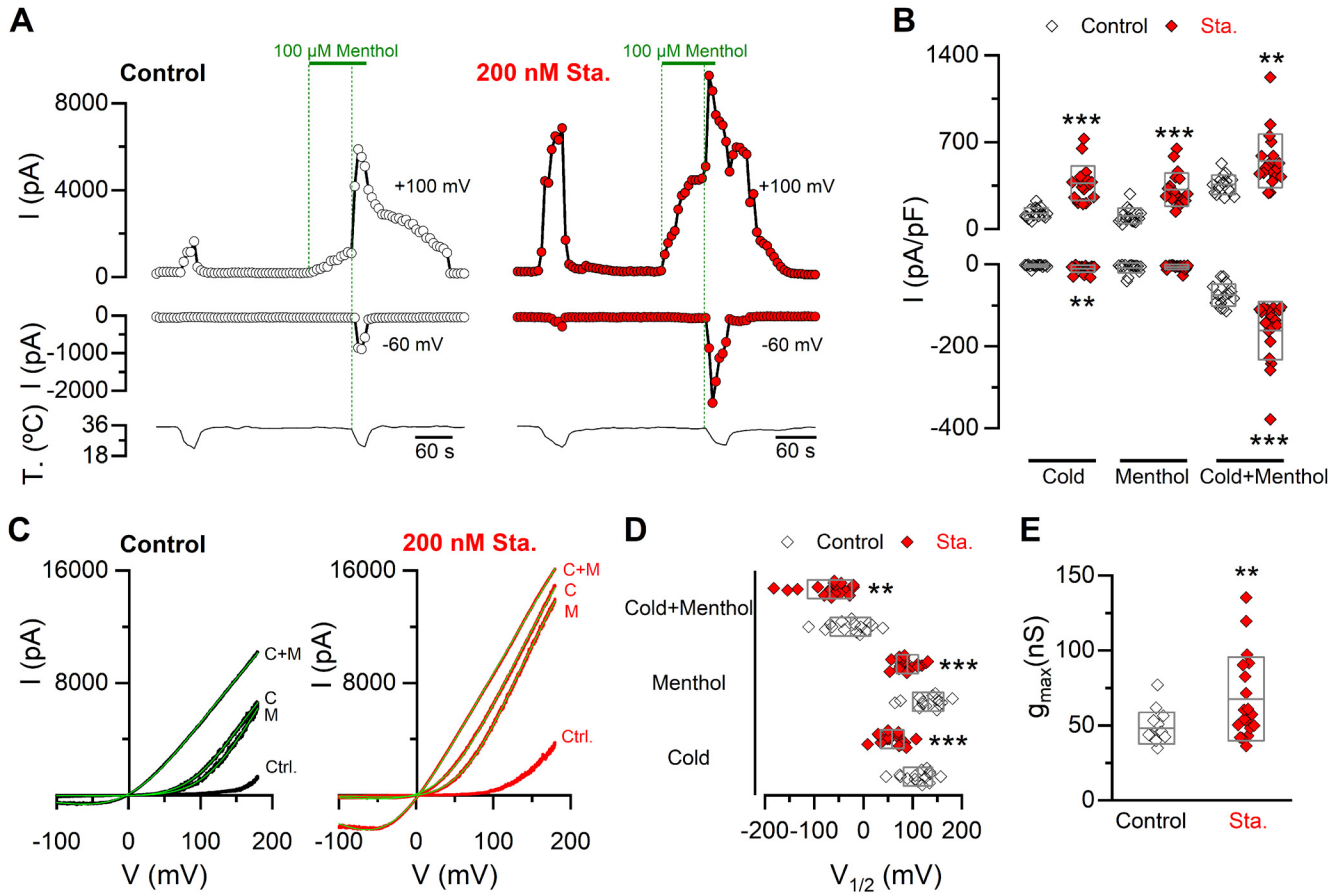

Figure 3. Inhibition of kinase activity induces a shift in the $V_{1/2}$ of TRPM8 toward negative membrane potentials and an increase in the g_{max}. ***A***, Representative recordings of whole-cell currents measured at 100 and −60 mV in a stable mTRPM8-myc expressing HEK293 cell line in control condition (open circles) or preincubated for 10-15 min with 200 nM staurosporine (Sta.) (red circles). ***B***, Scatter plots with mean and SD of maximal current density at 100 and −60 mV. Statistical significance was assessed with a two-tailed unpaired Student's *t* test with Welch's correction ($Cold_{100mV}$: $t_{(23)} = 7.11$, $p < 0.0001$; $Menthol_{100mV}$: $t_{(26)} = 6.08$, $p < 0.0001$; $Cold+menthol_{100mV}$: $t_{(23)} = 3.57$, $p = 0.0016$; $Cold_{-60mV}$: $t_{(24)} = 3.18$, $p = 0.0041$; $Menthol_{-60mV}$: $t_{(19)} = 0.72$, $p = 0.4819$; $Cold+menthol_{-60mV}$: $t_{(24)} = 4.93$, $p < 0.0001$). ***C***, *I–V* relationships in Control (Ctrl.), Cold (C), Menthol (M), and Cold+menthol (C + M) of cells in ***A***. Superimposed green line on each trace indicates the fit of the current to Equation 1 (see Materials and Methods). ***D***, Scatter plots with mean and SD of the $V_{1/2}$ values in the presence of the different agonists. ***E***, Scatter plots represent mean and SD g_{max} values estimated in the Cold+menthol condition. Statistical significance was assessed with a two-tailed unpaired Student's *t* test with Welch's correction: $V_{1/2}$ Cold: $t_{(26)} = 5.63$, $p < 0.0001$; $V_{1/2}$ Menthol: $t_{(24)} = 4.45$, $p = 0.0002$; $V_{1/2}$ Cold+menthol: $t_{(31)} = 2.88$, $p = 0.0071$; g_{max}: $t_{(24)} = 2.80$, $p = 0.0099$. $^{**}p < 0.01$. $^{***}p < 0.001$. $n > 15$ cells for each condition.

intracellular signaling pathways. The protocol entailed the fast cooling of the bath solution from ~35–34°C to 19°C, followed by the application of 100 μM menthol at 34°C, and finally combined with a second cold pulse to elicit maximal channel activity (Fig. 2*A*). Control responses were compared with those obtained after different incubation times (5, 10, and 20 min) with 200 nM staurosporine. Preincubating HEK293-mTRPM8-myc cells for 5 min with the kinase inhibitor is sufficient to robustly enhance cold- and menthol-evoked TRPM8 responses (Fig. 2*B*). The increase in amplitude was also accompanied by a shift in temperature threshold toward warmer temperatures. However, the maximal shift in temperature threshold was reached after 10 min of treatment (5 min ΔT. threshold = 0.9 ± 0.2°C***, $n = 95$; 10 min ΔT. threshold = 2.7 ± 0.1°C, $n = 89$; 20 min ΔT. threshold = 1.8 ± 0.2°C**, $n = 92$; one-way ANOVA test ($F_{(3,502)} = 62.67$, $p < 0.0001$), in combination with a Tukey's *post hoc* test: $^{**}p < 0.01$; $^{***}p < 0.001$, compared with 10 min). To find out whether constitutive kinase activity played a role under nonstimulated conditions in a cellular context that is closer to the native TRPM8 channel expression, we also examined responses in F11 DRG hybridoma cells. This cell line expresses functional TRPM8 channels responding to high menthol concentrations (500 μM) (Toro et al., 2015). However, using the protocol shown in Figure 2*A*, we did not observe Ca^{2+} responses to any of the stimuli applied, suggesting low levels of TRPM8 expression (data not shown). Therefore, we transfected F11 cells with mouse TRPM8-YFP, a fully functional channel with YFP tagged at the C-terminus (Pertusa et al., 2014). Although F11 cells expressing mTRPM8-YFP required longer incubation times with staurosporine, compared with HEK293-mTRPM8-myc cells, an equivalent potentiation in TRPM8-dependent responses occurred after 20 min of treatment (Fig. 2*C*,*D*).

Next, to further characterize the potentiation of cold- and menthol-evoked responses induced by kinase inhibition, we used whole-cell patch-clamp recordings of TRPM8 currents in HEK293-mTRPM8-myc cells. From a holding potential of −60 mV, channel activation was monitored with voltage ramps from −100 to 180 mV during agonist application (Fig. 3*A*,*C*). In close agreement with Ca^{2+} imaging results, preincubation with staurosporine increased the amplitude of currents elicited by cold and menthol. We also noticed a marked potentiation when both stimuli were applied simultaneously (Fig. 3*A*,*B*). TRPM8 gating is voltage-dependent, and activation by cold and menthol is linked to a shift in the voltage-activation

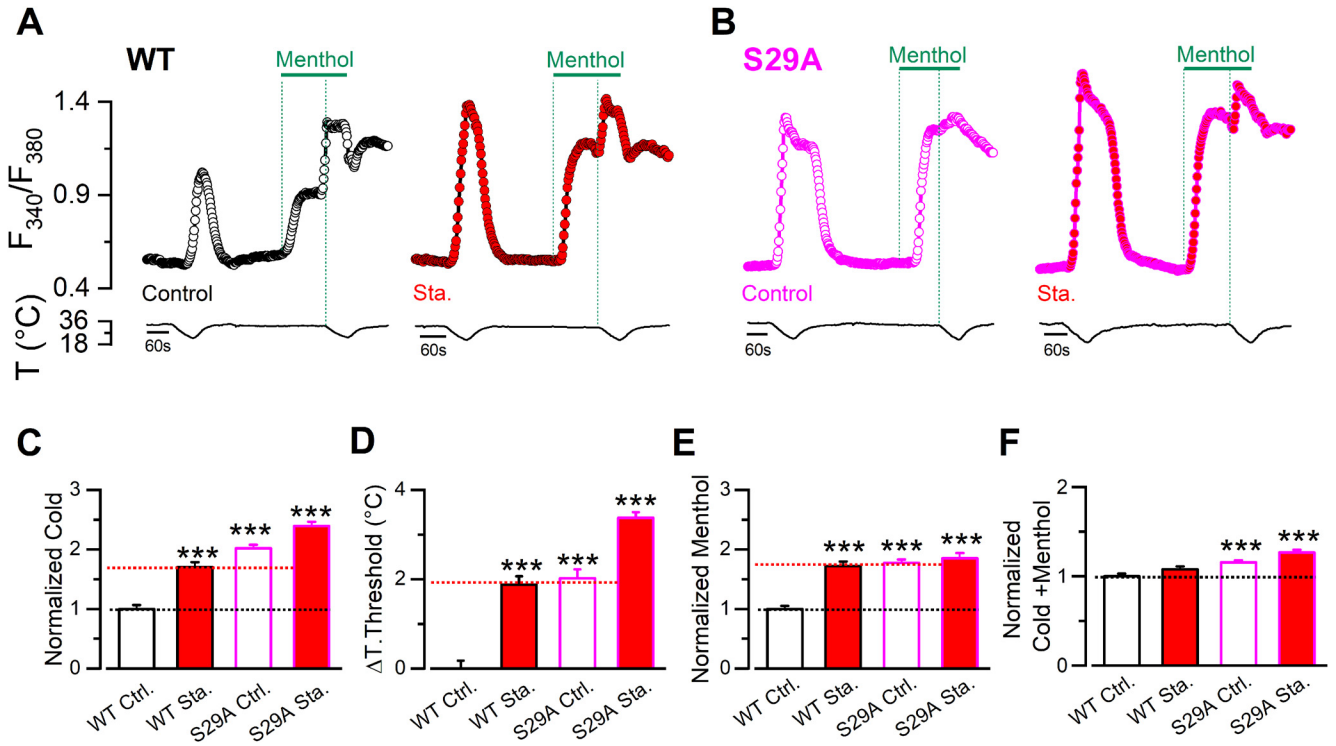

Figure 4. Phosphorylation of S29 residue constitutively modulates TRPM8 function. ***A***, Time course of $[Ca^{2+}]_i$ (F_{340}/F_{380}) responses in cells submitted to an experimental protocol that consists of a cold pulse, 100 μM menthol, and a combined stimulus of cold and menthol. Traces correspond to the Ca^{2+} signal of HEK293 cells transfected with WT mTRPM8-myc channel in control conditions (open black circles) and after a preincubation of 10 min with staurosporine 200 nM (red circles). ***B***, Same protocol in cells expressing S29A mutants in control conditions (open magenta circles) and treated with staurosporine (magenta circles filled with red). ***C-F***, Mean and SEM of cold response (***C***), ΔT. Threshold (***D***), Menthol- (***E***), and Cold+menthol-induced responses (***F***) in control conditions or after a 10 min incubation with 200 nM staurosporine (Sta.), of cells expressing WT channels or the unphosphorylated mutant. The values were normalized to the mean response observed in cells expressing WT channels in control conditions in parallel experiments. ***C***, The temperature threshold shift is shown compared with the WT in control conditions values. Positive values indicate shifts to warmer temperatures (WT Ctrl., $n = 105$; WT Sta., $n = 104$; S29A Ctrl., $n = 187$; S29A Sta., $n = 167$). Statistical analysis was performed using the one-way ANOVA test (Cold S29A: $F_{(3,559)} = 64.87$, $p < 0.0001$; ΔT. threshold S29A: $F_{(3,559)} = 53.04$, $p < 0.0001$; Menthol S29A: $F_{(3,559)} = 24.31$, $p < 0.0001$; Cold+menthol S29A: $F_{(3,559)} = 16.01$, $p < 0.0001$), in combination with a Dunnett's *post hoc* test: ***$p < 0.001$, compared with the control.

curve toward more negative (and physiologically relevant) membrane potentials (Brauchi et al., 2004; Voets et al., 2004; Mälkiä et al., 2007). To estimate the midpoint of activation ($V_{1/2}$) and the maximal conductance (g_{max}), the current traces derived from the voltage ramps were fitted with a Boltzmann-linear function (see Materials and Methods) (Fig. 3*C*). The enhanced cold and menthol responses induced by staurosporine treatment can be explained by changes in gating that involve a large shift in the voltage dependence curve of ~50 mV toward more negative membrane potentials (Fig. 3*D*), and a ~40% increase in the g_{max} value, suggesting a higher number of TRPM8 channels at the cell surface (Fig. 3*E*).

Collectively, these results suggest that basal phosphorylation downregulates TRPM8 function, altering its biophysical properties and probably reducing the availability of functional channels at the plasma membrane.

Phosphorylation of residue S29 is a key modulator of TRPM8 function

Serines 26, 29, 541, and 542 detected in our spectrometry analysis of phosphorylated residues are within regions of the intracellular N-terminal domain of TRPM8 known to regulate its function (Pertusa et al., 2014, 2018). Previously, we found that deletions or substitutions in the first 40 amino acids of TRPM8, where S26 and S29 are located, yielded channels with augmented responses to agonists (Pertusa et al., 2014). Moreover, cells expressing these TRPM8 constructs displayed temperature thresholds shifted by 2°C toward warmer temperatures (Pertusa et al., 2014), analogous to the staurosporine effects on WT channels (see Fig. 2*B*). Serines at positions 541 and 542 are within a 30 amino acid stretch in the proximal N-terminus, where substitutions in this sequence also increase cold and menthol responses in the resulting mutant channels (Pertusa et al., 2018). Because pharmacological inhibition of kinase activity and mutations within these regions rendered channels with similarly enhanced cold- and menthol-evoked responses, we hypothesized that basal phosphorylation of some of these serines could determine TRPM8 functional properties under resting conditions. To test this hypothesis, we systematically mutated serines 26, 29, 541, and 542 to alanines, and used Ca^{2+} imaging to probe channel function. We compared the responses of cells expressing mTRPM8 WT channels with those for each mutant in control conditions and after a 10 min preincubation with 200 nM staurosporine. The key result of this functional screening is shown in Figure 4. Cells expressing the single-point mutant S29A exhibited a strong potentiation of cold and menthol responses under basal conditions (Fig. 4*A*,*B*). This potentiation was very similar to the one observed in WT channels after staurosporine treatment. In contrast, incubation of S29A mutants with the kinase inhibitor produced a modest but significant potentiation to cold ($\Delta F_{340}/F_{380}$ S29A Ctrl.: 0.57 ± 0.02, $n = 187$; vs $\Delta F_{340}/F_{380}$ S29A staurosporine: 0.70 ± 0.02, $n = 167$; $t_{(315)} = 4.44$, $p < 0.0001$, unpaired *t* test with Welch's correction) (Fig. 4*C*), accompanied by a shift in thermal threshold toward a warmer temperature (S29A Ctrl.: 26.9 ± 0.2°C, $n = 187$; vs S29A staurosporine: 28.3 ± 0.1°C, $n =$

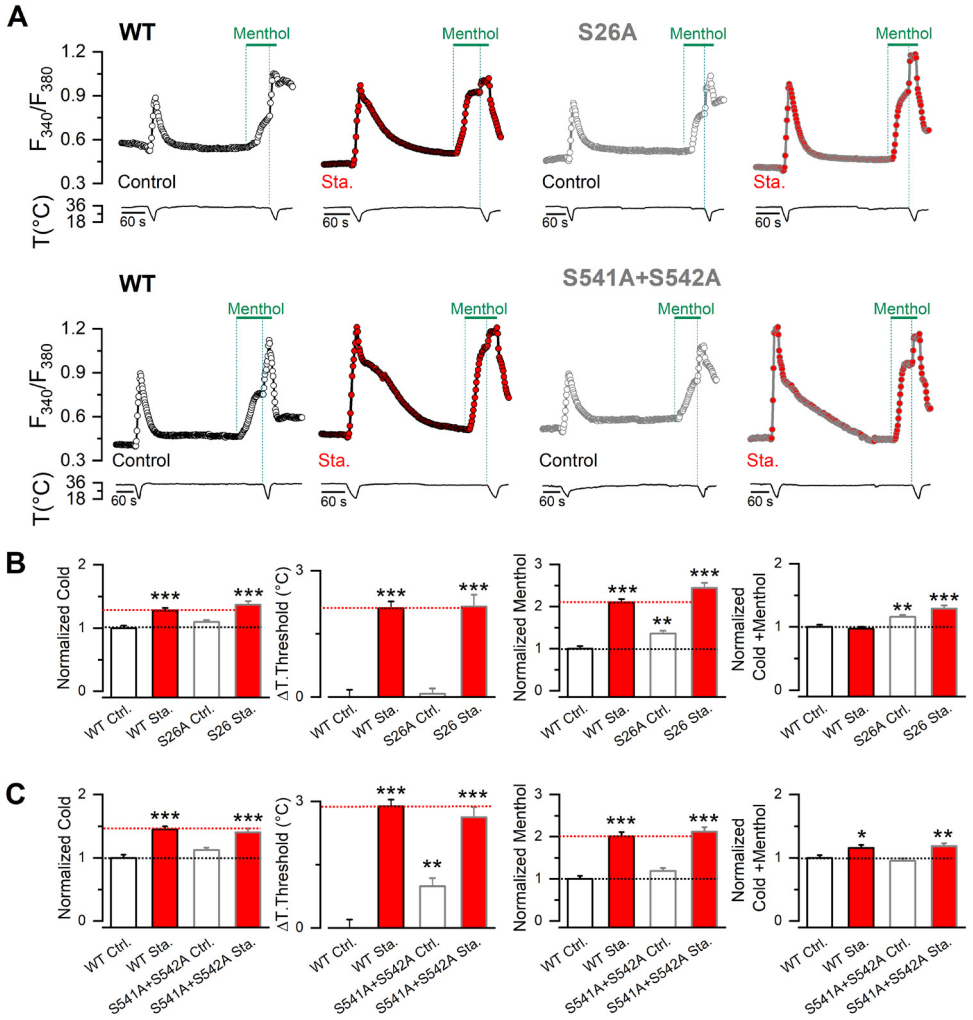

Figure 5. S26A and S541A+S542A showed minor alterations in their responses to TRPM8 agonists. ***A***, Time course of $[Ca^{2+}]_i$ (F_{340}/F_{380}) of cells submitted to an experimental protocol that consists of a cold pulse, 100 μM menthol, and a combined stimulus of cold and menthol. For each mutant channel displayed, the traces correspond to the Ca^{2+} signal of HEK293 cells transfected with WT mTRPM8-myc channel in control conditions (open black circles) and after a preincubation of 10 min with 200 nM staurosporine (Sta.) (red circles), and transfected with S26A and S541A+S542A mutants in control conditions (open gray circles) and treated with staurosporine (gray circles filled with red). ***B***, ***C***, Plots represent the mean and SEM of cold response, ΔT. Threshold, Menthol-, and Cold+menthol-induced responses of TRPM8 in control conditions or after a 10 min incubation with staurosporine 200 nM, of cells expressing WT channels or unphosphorylated mutants. The values were normalized to the mean response observed in control conditions in parallel experiments. ΔT. Threshold represents the temperature threshold shift displayed according to the mTRPM8-myc values. Positive values indicate shifts to warmer temperatures (***B***: WT Ctrl., $n = 108$ WT, Sta., $n = 107$; S26A Ctrl., $n = 249$; S26A Sta., $n = 85$; ***C***: WT Ctrl., $n = 89$ WT Sta., $n = 122$; S541A+S542A Ctrl., $n = 113$; S541A+S542A Sta., $n = 101$). Statistical analysis was performed using the one-way ANOVA test (Cold S26A: $F_{(3,545)} = 14.53$, $p < 0.0001$; ΔT. threshold S26A: $F_{(3,545)} = 45.40$, $p < 0.0001$; Menthol S26A: $F_{(3,545)} = 57.14$, $p < 0.0001$; Cold+menthol S26A: $F_{(3,545)} = 12.27$, $p < 0.0001$; Cold S541A+S542A: $F_{(3,421)} = 19.22$, $p < 0.0001$; ΔT. threshold S541A+S542A: $F_{(3,421)} = 46.42$, $p < 0.0001$; Menthol S541A+S542A: $F_{(3,421)} = 36.05$, $p < 0.0001$; Cold+menthol S541A+S542A: $F_{(3,421)} = 7.16$, $p = 0.0001$), in combination with a Dunnett's *post hoc* test: *$p < 0.05$; **$p < 0.01$; ***$p < 0.001$; compared with the control.

167; $t_{(305)} = 5.13$, $p < 0.0001$, unpaired *t* test with Welch's correction) (Fig. 4*D*). However, S29A response to menthol was unaffected by the treatment (Fig. 4*E*).

Unlike S29A, S26A and S541A+S542A mutants behaved similarly to WT channels (Fig. 5). In the case of S26A, cold-evoked responses and thermal threshold were indistinguishable from those observed in WT channels; only menthol application evoked a slightly larger response. The double mutant S541A+S542A showed only a minimal shift in thermal threshold toward warmer temperatures. In both cases (S26A and S541A+S542A), staurosporine treatment induced a potentiation of cold- and menthol-evoked responses comparable to that observed in WT channels (Fig. 5).

These results show that, among the four phosphorylated amino acids identified by MS within the N-terminal domain, S29 is the residue that contributes most to the modulation of TRPM8 function by basal phosphorylation.

Whole-cell patch-clamp recordings of the S29A mutant confirmed the alterations in TRPM8 activity suggested by the Ca^{2+} imaging results. As shown in Figure 6*A–C*, mutant channels exhibited a robust potentiation of cold and menthol-evoked responses under basal conditions compared with WT channels. Moreover, analysis of the *I–V* curves revealed a shift in the $V_{1/2}$ toward negative potentials and an increase in the g_{max} (Fig. 6*D*,*E*). These changes were comparable to those observed after incubating WT TRPM8-expressing HEK293 cells with the kinase inhibitor (see Fig. 3*D*,*E*), indicating that S29 is involved in the two main molecular mechanisms underlying TRPM8 downregulation by basal phosphorylation.

The incubation of S29A mutants with staurosporine was informative. Largely, this mutation occluded its potentiating

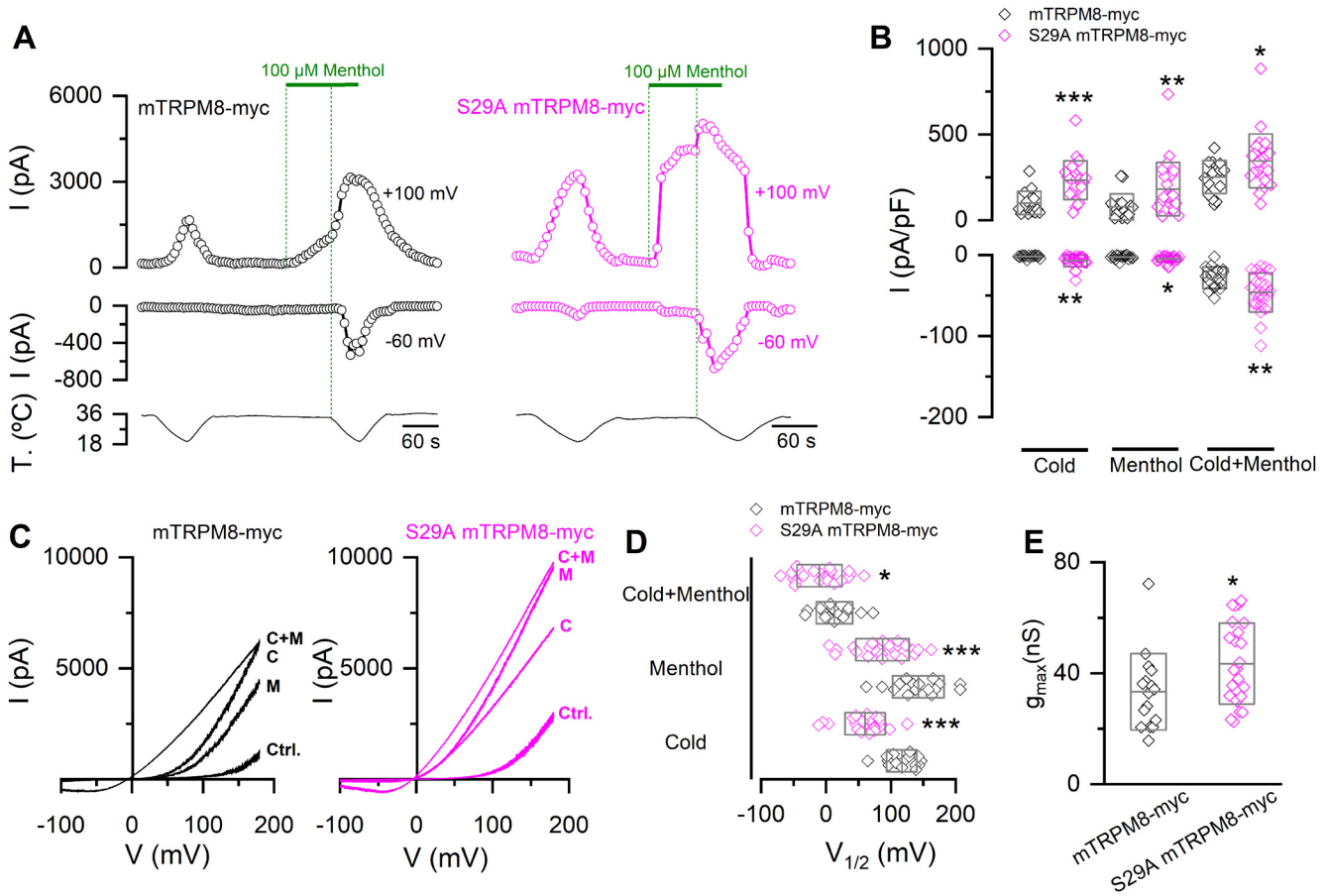

Figure 6. The S29A mutant recapitulates the alterations in the biophysical phenotype induced by kinase activity inhibition. ***A***, Representative recordings of whole-cell currents measured at 100 and −60 mV in HEK293 transfected with mTRPM8-myc (open black circles) and S29A mTRPM8-myc (open magenta circles) channels. ***B***, Scatter plots with mean and SD of maximal current density at 100 and −60 mV. Statistical significance was assessed with a two-tailed unpaired Student's *t* test with Welch's correction ($Cold_{100mV}$: $t_{(37)} = 4.64$, $p < 0.0001$; $Menthol_{100mV}$: $t_{(35)} = 2.79$, $p = 0.0086$; $Cold+menthol_{100mV}$: $t_{(37)} = 2.35$, $p = 0.0241$; $Cold_{-60mV}$: $t_{(25)} = 3.54$, $p = 0.0016$; $Menthol_{-60mV}$: $t_{(37)} = 2.18$, $p = 0.0357$; $Cold+menthol_{-60mV}$: $t_{(37)} = 3.02$, $p = 0.0046$). ***C***, *I–V* relationships in Control (Ctrl.), Cold (C), Menthol (M), and Cold+menthol (C + M) conditions of cells in ***A***. ***D***, Scatter plots with mean and SD of the $V_{1/2}$ values. ***E***, Scatter plots with mean and SD g_{max} values estimated in Cold+menthol condition. Statistical significance was assessed with a two-tailed unpaired Student's *t* test with Welch's correction ($V_{1/2}$ cold: $t_{(37)} = 6.58$, $p < 0.0001$; $V_{1/2}$ menthol: $t_{(33)} = 4.23$, $p = 0.0002$; $V_{1/2}$ Cold+menthol: $t_{(33)} = 2.23$, $p = 0.0325$; g_{max}: $t_{(33)} = 2.22$, $p = 0.0334$). *$p < 0.05$; **$p < 0.01$; ***$p < 0.001$; $n > 15$ cells for each condition.

effects (Fig. 7). The use of a broad kinase inhibitor implies that we cannot establish whether its impact on TRPM8 modulation is direct or indirect. However, the fact that the staurosporine effect is nearly abrogated for this specific mutation suggests that kinase inhibition and the unphosphorylation of S29 converge in a common point of this regulatory pathway. The only difference was a modest increase in cold-evoked responses (Fig. 7*A–C*), caused by a shift of the voltage activation curve in cold conditions toward more negative membrane potentials (Fig. 7*D*), suggesting that, in addition to phosphorylation of serine 29, the phosphorylation of other residues could also contribute to the regulation of TRPM8 thermal responses. Importantly, staurosporine treatment in cells transfected with the S29A mutant did not produce significant changes in the g_{max} value, supporting the unique contribution of S29 to the regulation of functional TRPM8 expression at the plasma membrane (Fig. 7*E*).

Inhibition of basal phosphorylation increases the number of active TRPM8 channels at the plasma membrane

The increase in the g_{max} values after staurosporine incubation (see Fig. 3*E*) suggested a higher number of TRPM8 channels at the cell surface. To test this hypothesis, we performed nonstationary noise analysis, a technique that estimates the number of active channels at the plasma membrane from fits of the current variance against the mean current (Alvarez et al., 2002). As indicated in Figure 8, under control conditions, HEK293-mTRPM8-myc cells expressed 604 ± 66 channels, and the estimated unitary current at 19°C was ~50 pS, values in line with previous reports (Pertusa et al., 2012, 2018; Rivera et al., 2020). In contrast, preincubation with staurosporine increased the number of channels significantly, to a mean of 1049 ± 159, without changes in the mean unitary conductance (Fig. 8*A–C*).

To follow the dynamics of the recruitment of TRPM8 channels to the cell surface in a noninvasive manner, we used TIRF microscopy. This optical technique allows the monitoring of fluorophores located in a ~200 nm optical section near the cell surface. To this end, we transfected COS-7 cells with mTRPM8-YFP and S29A-mTRPM8-YFP constructs, evaluating TIRF under control conditions or during the application of 200 nM staurosporine. During treatment with the kinase inhibitor, cells displayed a progressive increase in their basal fluorescence that amounted to an ~70% increase (1.70 ± 0.20 times) after 16 min. In contrast, cells incubated with vehicle (DMSO) showed no significant change in the F/F_0 ratio (1.10 ± 0.04 times) over the same period (Fig. 8*D–F*). The increase in TIRF fluorescence

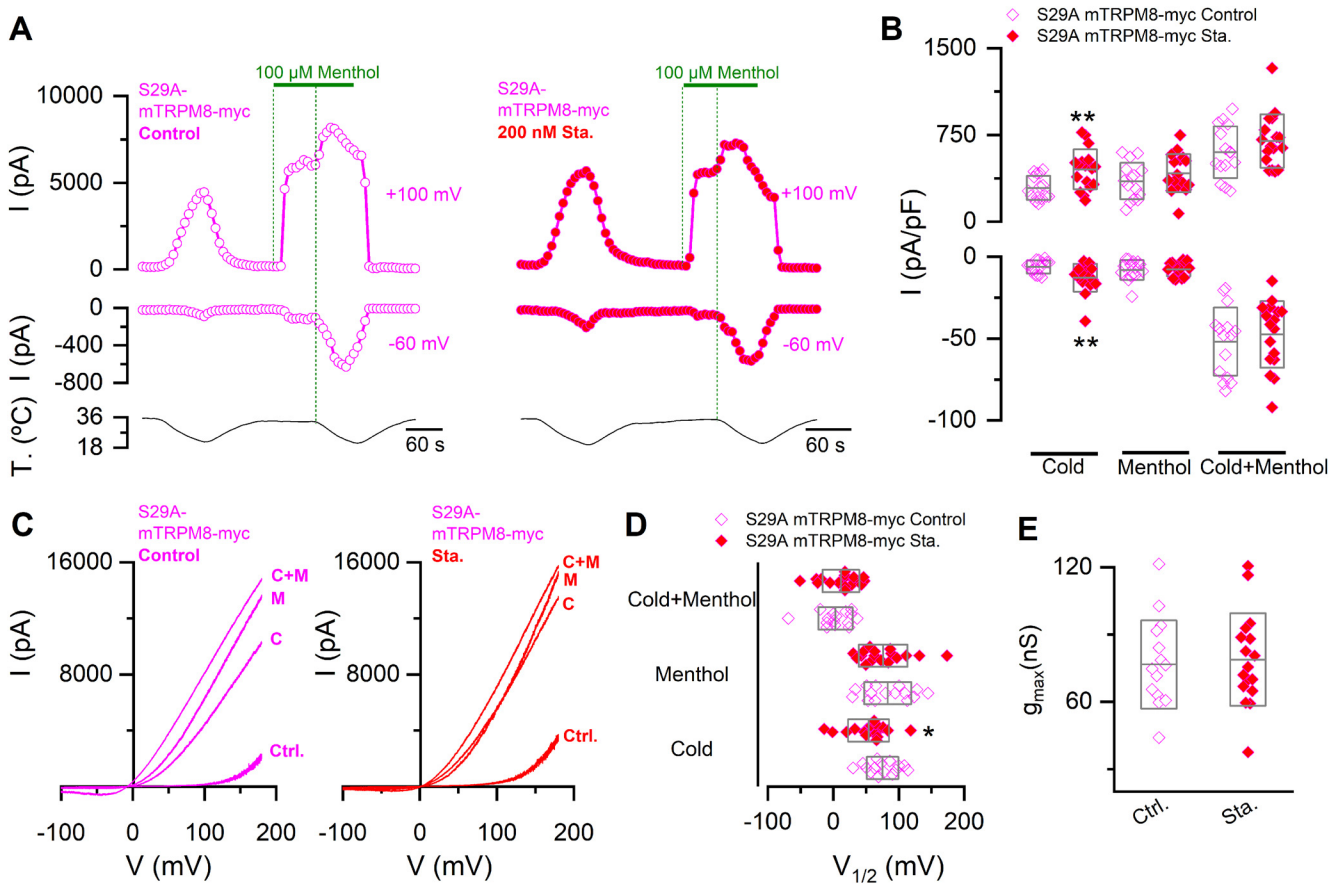

Figure 7. The S29A mutant shows reduced sensitivity to kinase inhibition. ***A***, Representative recordings of whole-cell currents measured at 100 and −60 mV in HEK293 cells transfected with S29A mTRPM8-myc mutant in control condition (open magenta circles) or preincubated for 10-15 min with 200 nM staurosporine (red magenta circles). ***B***, Scatter plots with mean and SD of maximal current density at 100 and −60 mV. Statistical significance was assessed with a two-tailed unpaired Student's *t* test with Welch's correction ($Cold_{100mV}$: $t_{(26)} = 3.21$, $p = 0.0035$; $Menthol_{100mV}$: $t_{(29)} = 1.18$, $p = 0.2470$; $Cold+menthol_{100mV}$: $t_{(29)} = 1.19$, $p = 0.2419$; $Cold_{-60mV}$: $t_{(23)} = 2.86$, $p = 0.0088$; $Menthol_{-60mV}$: $t_{(24)} = 0.19$, $p = 0.8469$; $Cold+menthol_{-60mV}$: $t_{(29)} = 0.60$, $p = 0.5506$). ***C***, *I–V* relationships in Control (Ctrl.), Cold (C), Menthol (M), and Cold+menthol (C + M) conditions of cells in ***A***. ***D***, Scatter plots with mean and SD of the $V_{1/2}$ values. ***E***, Scatter plots with mean and SD g_{max} values estimated in the Cold+menthol condition. Statistical significance was assessed with a two-tailed unpaired Student's *t* test with Welch's correction ($V_{1/2}$ Cold: $t_{(29)} = 2.18$, $p = 0.0377$; $V_{1/2}$ Menthol: $t_{(29)} = 0.55$, $p = 0.5870$; $V_{1/2}$ Cold+menthol: $t_{(29)} = 0.88$, $p = 0.3875$; g_{max}: $t_{(29)} = 0.30$, $p = 0.7625$). *$p < 0.05$. **$p < 0.01$. $n > 14$ cells for each condition.

turned statistically significant after 9 min of incubation with the staurosporine (Fig. 8*E*), reinforcing the idea that the dephosphorylation of TRPM8 alters the dynamics of its trafficking, increasing the population of channels close to the cell surface. In agreement with the electrophysiological results described previously, cells expressing the S29A-mTRPM8-YFP mutant did not show alterations in their TIRF fluorescence after staurosporine incubation (Fig. 8*G–I*), strongly suggesting that S29 phosphorylation participates in the regulation of TRPM8 abundance at the plasma membrane.

Regulation of TRPM8-dependent currents by kinase activity in CTNs

Next, we asked whether the TRPM8 modulation induced by the pharmacological suppression of kinase activity could also be observed in a more physiological context. To this end, cultured mouse trigeminal neurons were preincubated for 10 min with 200 nM staurosporine or vehicle, and CSNs were identified by their $[Ca^{2+}]_i$ rise during a cooling ramp (Madrid et al., 2009; Piña et al., 2019) (Fig. 9*A*). As described previously (Madrid et al., 2009), the thermal threshold of CTNs varies over a wide range. No differences were observed in the mean temperature threshold in these two conditions (threshold control: 29.1 ± 0.5°C, $n = 49$ vs staurosporine: 28.6 ± 0.4°C, $n = 48$; $t_{(95)} = 0.7785$, $p = 0.4382$, unpaired Student's *t* test) (Fig. 9*B*). However, the brief treatment of cultured TG neurons with staurosporine increased the percentage of CSNs (13.2%, $n = 49$ of 370 in control conditions, vs 20.3%, $n = 48$ of 237 treated neurons; $p = 0.0234$, Fisher's exact test) (Fig. 9*C*), suggesting the recruitment of a subpopulation of former cold-insensitive neurons (CINs) that became cold-sensitive because of functional upregulation of TRPM8. After identifying CSNs by Ca^{2+} imaging, direct measurement of functional TRPM8 channels was obtained using whole-cell voltage-clamp recordings at −60 mV. We used stimulation with cold (I_{cold}), 1 µM WS-12 (a selective agonist of TRPM8 channels) (Bödding et al., 2007) ($I_{WS\text{-}12}$), and a combination of cold plus the TRPM8 activator ($I_{cold+WS\text{-}12}$) to reach maximal channel activation in CSNs (Fig. 9*D*). On average, I_{cold}, $I_{WS\text{-}12}$, and $I_{cold+WS\text{-}12}$ were larger in CSNs treated with staurosporine compared with control neurons (Fig. 9*E*).

We also investigated the responses of TRPM8-positive cold thermoreceptors using a double-pulse protocol, wherein we compared the basal response to cold before and after treatment with 200 nM staurosporine in the same neuron (Fig. 10). After washout of the kinase inhibitor, we performed a second cold stimulus and compared the amplitude of the responses as a ratio of Cold 2/Cold 1 (Fig. 10*A*,*B*). To corroborate the expression of

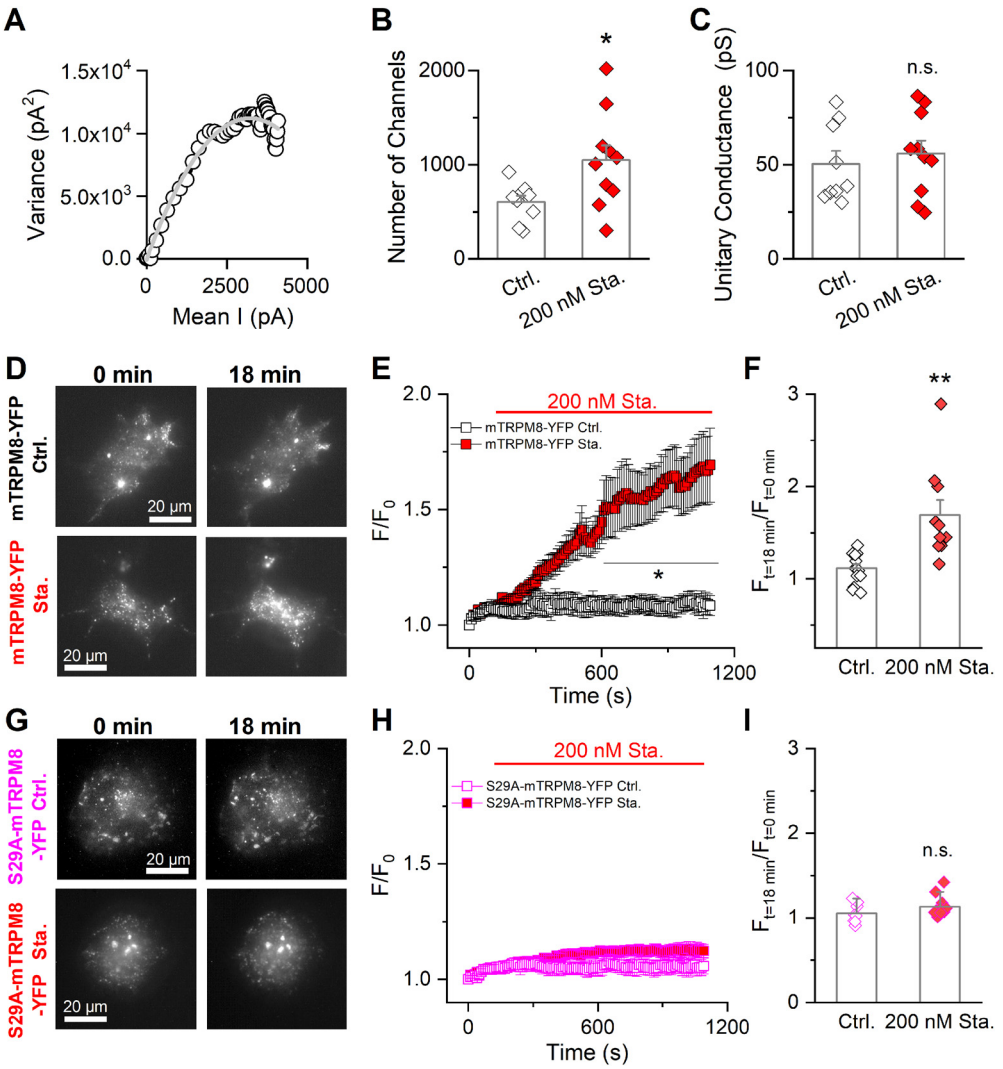

Figure 8. Basal phosphorylation is a key modulator of TRPM8 levels at the plasma membrane. ***A***, Nonstationary noise analysis. Scatter plot of variance versus mean current obtained from whole-cell currents of a stable mTRPM8-myc expressing HEK293 cell in control conditions (open black circles). Current records were collected during activation of the channels by 150 ms depolarizing voltage steps from 0 to 180 mV, at 19°C. Solid gray line is a parabola that best fits the data (Eq. 2). ***B***, ***C***, Bar graph represents mean and SEM and data points of the number of active channels (***B***) and unitary conductance (***C***) in the control condition and in cells pretreated for 10-15 min with staurosporine. Statistical significance was assessed with a two-tailed unpaired Student's *t* test with Welch's correction (number of channels: $t_{(11)} = 2.57$, $p = 0.0260$; unitary conductance: $t_{(17)} = 0.78$, $p = 0.4458$; $n > 8$ cells for each condition). ***D***, Representative TIRF images of COS-7 cells expressing mTRPM8-YFP at t_0 and t_{18} in control conditions and after staurosporine treatment. ***E***, Quantification of total TIRF fluorescence intensity during application of control extracellular solution with vehicle (DMSO) (black squares) or extracellular solution supplemented with 200 nM staurosporine (red squares). The fluorescent intensities are normalized to the intensity values at t_0. Data are mean ± SEM. A two-way ANOVA was used to assess statistical significance: $^*p < 0.05$, significance of the Bonferroni's *post hoc* test comparing control cells with staurosporine treatment. ***F***, Bar graph represents the mean and SEM and data points of the TIRF fluorescence ratio between $t_{18\ min}$ and t_0. Statistical significance was assessed with a two-tailed unpaired Student's *t* test with Welch's correction ($t_{(10)} = 3.47$, $p = 0.0060$; mTRPM8-YFP Ctrl., $n = 14$; mTRPM8-YFP Sta., $n = 10$). ***G-I***, Same as in ***D-F*** in COS-7 cells transfected with S29A TRPM8-YFP mutant. Statistical significance was assessed with a two-tailed unpaired Student's *t* test: $t_{(17)} = 1.40$, $p = 0.1789$; S29A-mTRPM8-YFP Ctrl., $n = 8$; S29A-mTRPM8-YFP Sta., $n = 11$; ns, $p > 0.05$; $^*p < 0.05$; $^{**}p < 0.01$.

TRPM8 in the neurons responding to cold, we also applied a pulse of 1 µM of WS-12 after the second cold stimulus followed by a third cooling ramp in the presence of this TRPM8 activator (Fig. 10*A*). As shown in Figure 10*B*, neurons in the control condition showed a decrease in the amplitude of the second response to cold, most probably because of channel desensitization (Rohacs et al., 2005; Mälkiä et al., 2007; Yudin et al., 2011). However, this reduction was strongly diminished in cells treated with staurosporine, resulting in an amplitude ratio closer to 1. Moreover, kinase inhibition also produced a 1.1 ± 0.2°C shift in the temperature activation threshold to higher temperatures. In contrast, nontreated neurons showed a 0.4 ± 0.3°C shift in their mean temperature threshold to lower temperatures (Fig. 10*C*). This protocol allowed us to assess the change in thermal sensitivity in the same neuron after the treatment with staurosporine, unveiling a shift that was masked when averaging results obtained from neurons with different thresholds (see Fig. 9*B*). Interestingly, in addition to TRPM8-expressing CTNs, we also found cold-insensitive WS-12-sensitive neurons that were recruited as cold-sensitive after kinase inhibition during the second cold pulse (mean T. threshold 24.6 ± 0.9°C, $n = 3$; data not shown), an observation that is in line with the increase in the population size of CSNs described previously (see Fig. 9*C*). Thus, these findings suggest that the functional upregulation of TRPM8 channels induced by inhibition of kinase activity strongly potentiates cold-sensitivity of trigeminal primary sensory neurons.

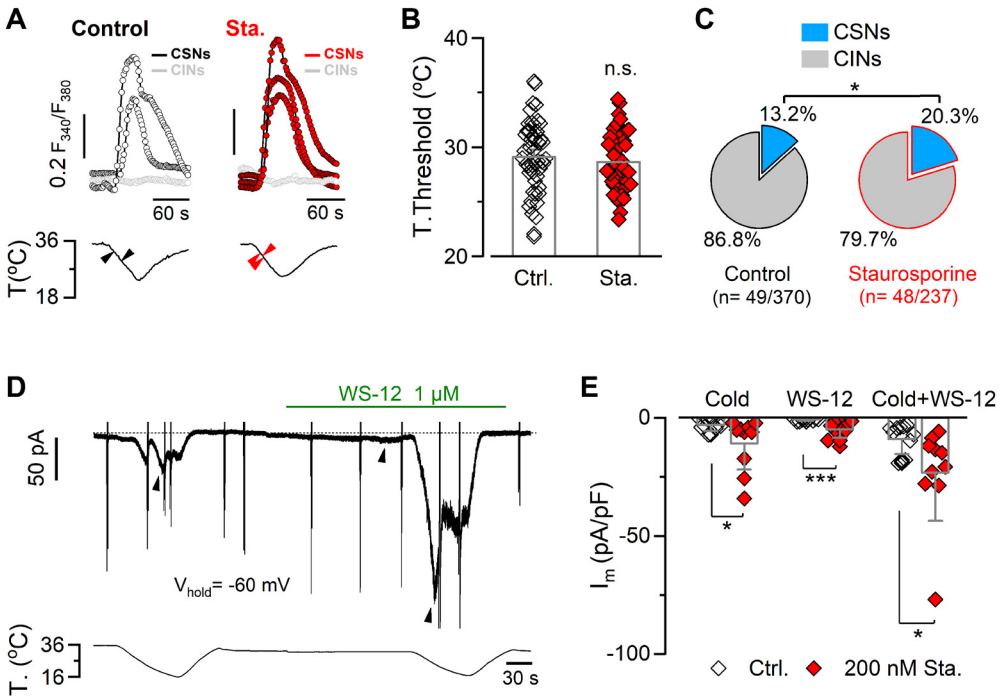

Figure 9. Kinase inhibition potentiates TRPM8-dependent currents in trigeminal primary sensory neurons. ***A***, Ratiometric $[Ca^{2+}]_i$ responses to cooling (top panels) of CSNs and CINs from mouse TG in control conditions and after 10 min treatment with 200 nM staurosporine, recorded simultaneously with the temperature of the bath (bottom panels). Black and red arrowheads on the temperature traces correspond to the thermal thresholds of CTNs in the top panels. ***B***, Bar graph represents the mean and SEM and data points of temperature threshold exhibited by CSNs in control conditions or preincubated with 200 nM staurosporine. Statistical significance was assessed with a two-tailed unpaired Student's *t* test ($t_{(95)} = 0.7785$, $p = 0.4382$; ns, $p > 0.05$; $n > 40$ neurons for each condition). ***C***, Pie plots represent the percentage of CSN and CIN populations of trigeminal neurons treated or not with staurosporine. Size populations were compared using Fisher's exact test ($p = 0.0234$). ***D***, Simultaneous recording of whole-cell current (top) and bath temperature (bottom) during two consecutive cooling ramps combined with the application of WS-12 (1 μM) in a representative cold-thermoreceptor neuron in control condition ($V_{hold} = -60$ mV). The spike-like currents correspond to the truncated responses to voltage ramps from −100 to 120 mV (1100 ms duration) that were also applied in this particular neuron. Dotted line indicates the 0 holding current. ***E***, Bar graph represents the mean and SEM and individual data points of cold-, WS-12-, and cold+WS-12-induced current densities in cold thermoreceptor neurons in the control condition (gray bars plus open diamonds) and in neurons treated with staurosporine (gray bars plus red diamonds). Maximal current densities were measured at the peak of the response to each stimulus (black arrowheads in ***D***). Statistical significance was assessed with a Mann–Whitney test (I_{cold}, $U = 25$, $p = 0.0378$; $I_{Ws\text{-}12}$, $U = 2500$, $p = 0.0002$; $I_{cold+ws\text{-}12}$, $U = 19$, $p = 0.0124$; Ctrl., $n = 11$; Sta., $n = 10$). *$p < 0.05$. ***$p < 0.001$.

We also used a double-pulse protocol with two consecutive applications of WS-12 at a subsaturating concentration (Fig. 10*D*), to explore the responses of CTNs to this TRPM8 activator. Notably, treatment with the kinase inhibitor produced a ~30% potentiation of the second WS-12-evoked response, in contrast to the control condition where the WS-12 2/WS-12 1 ratio was near 0.9 (Fig. 10*E*).

Together, our results in trigeminal neurons are consistent with those obtained with the recombinant channel, supporting the hypothesis that basal kinase activity induces a negative modulation of TRPM8-dependent responses in the native context. Thus, this regulatory mechanism could contribute to fine-tune the cold sensitivity of primary sensory neurons expressing TRPM8 channels.

Mathematical modeling of cold thermoreceptor modulation by dephosphorylation of TRPM8

Staurosporine could affect several molecular targets in addition to TRPM8 phosphorylation, making the interpretation of observations made in neurons difficult. To overcome this limitation, we performed computer simulations using a conductance-based model implemented on cold thermoreceptors (Olivares and Orio, 2015; Olivares et al., 2015), testing the hypothesis that changes in TRPM8 basal phosphorylation state can produce alterations in CTN activity. In the model, sensitivity to temperature reductions is mainly because of a depolarizing cold- and voltage-dependent current (TRPM8-like), which generates large changes in the firing rate of cold thermoreceptors in response to temperature variations. We use the model to explore the effect of manipulating the g_{max} (g_{M8}) and $V_{1/2}$ values of TRPM8 conductance on the cold-evoked activity of CTNs (Fig. 11), emulating this channel function in a staurosporine-like (i.e., unphosphorylated S29 TRPM8) condition. We adjusted the model parameters to reproduce the behavior observed in cultured CTNs, displaying no spontaneous activity at basal temperature and a strong response of action potential firing when the temperature is decreased (Fig. 11*A*, left panels). As shown in Figure 11*A* (right panels), the parameter changes that emulate the staurosporine treatment (i.e., increase in g_{max} and leftward shift in $V_{1/2}$) caused the model neuron to start firing action potentials at a higher temperature (i.e., reduced thermal threshold), also reaching a higher maximum firing rate. To study this effect in a broader set of conditions and from a population perspective, we obtained a collection of responses in different parameter sets ("individuals"). Each of the individuals has a distinct threshold for cold-evoked activity, varying between 33.5°C and 18.5°C, and some do not respond to cooling up to 18°C (Fig. 11*B*, Control), mimicking the experimental findings in cultured trigeminal neurons (Madrid et al., 2009). When $V_{1/2}$ of TRPM8 activation is shifted 50 mV to more negative membrane potentials and its g_{max} value is increased by 40%, all individual thresholds shift toward higher temperatures, turning several high-threshold CTNs into low-threshold ones. The maximum firing rate on cooling also increased significantly (Fig. 11*C*), and the simulated cold-evoked TRPM8 current displays an increase comparable to

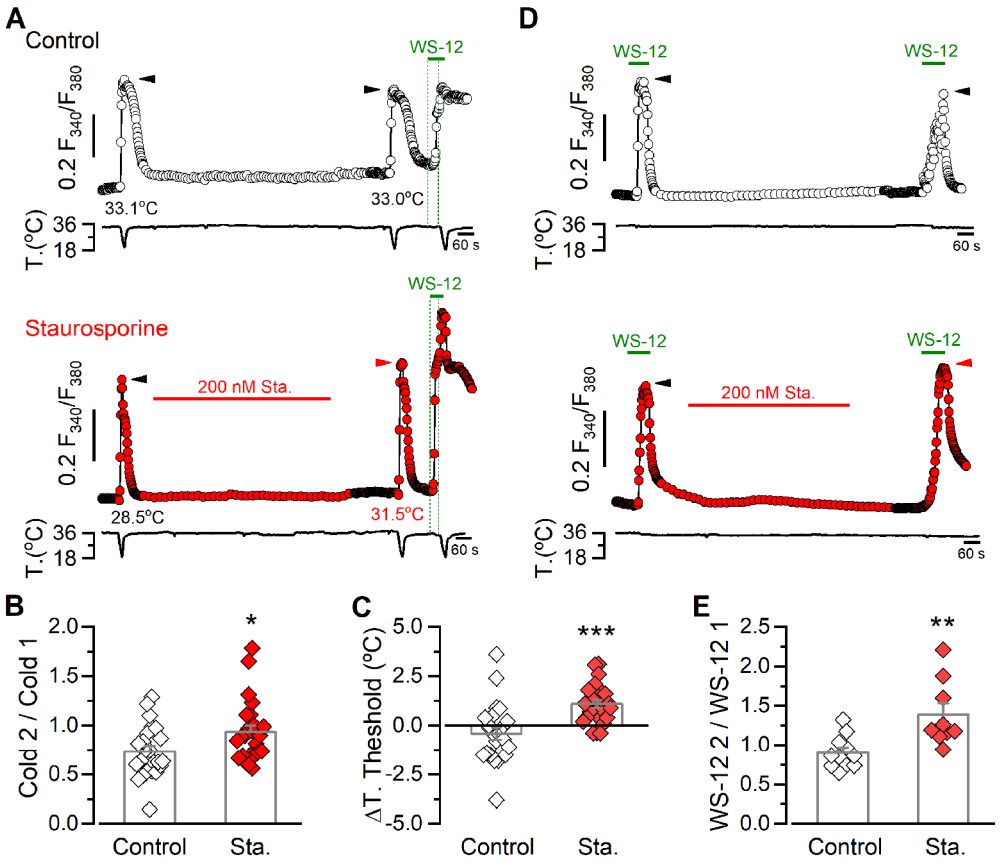

Figure 10. Kinase inhibition potentiates cold- and WS-12-evoked responses in trigeminal cold thermoreceptors. ***A***, Fura-2 ratiometric imaging of $[Ca^{2+}]_i$ responses to consecutive cooling ramps in TG CSNs, recorded simultaneously with the temperature of the bath. Traces are representative of a control experiment (top) and a CSN perfused with 200 nM staurosporine for 10 min (bottom). A 1 μM WS-12 stimulus followed by a cooling ramp in the presence of the TRPM8 activator was also applied to assess the expression of the channel in both cases. Green dotted lines indicate the start of the WS-12 application and of the third cold stimulus. Black and red arrows on the $[Ca^{2+}]_i$ traces indicate the maximal responses in each condition. Thermal thresholds of the neurons in response to the cold pulses are also indicated. ***B***, Bar graph and data points of the ratio of cold-evoked responses (Cold 1/Cold 2) in control and in CTNs treated with the kinase inhibitor. Statistical significance was assessed with a two-tailed unpaired Student's *t* test ($t_{(45)} = 2.364$, $p = 0.0224$; Control, $n = 23$, Sta., $n = 24$). ***C***, Bar graph and data points represent the shift in the temperature threshold during the second cooling stimulus (T. threshold 2, T. threshold 1). Negative values indicate shifts toward lower temperatures. Statistical significance was assessed with a two-tailed unpaired Student's *t* test with Welch's correction ($t_{(37)} = 3.956$, $p = 0.0003$; Control, $n = 23$, Sta., $n = 24$). Thermal thresholds in response to the first cold pulse were 29.8 ± 0.7°C in the control group ($n = 23$) and 30.0 ± 0.6°C in neurons that were treated with staurosporine ($n = 24$) ($t_{(45)} = 0.2815$, $p = 0.8280$, unpaired *t* test). The maximal response (ΔRatio F_{340}/F_{380}) evoked by the first cold pulse was 0.322 ± 0.04 ($n = 23$) and 0.318 ± 0.03 ($n = 24$) in both groups, respectively ($t_{(45)} = 0.0877$, $p = 0.9305$, unpaired *t* test). ***D***, Representative ratiometric $[Ca^{2+}]_i$ traces in TG CSNs, recorded simultaneously with the temperature of the bath, showing the response to two consecutive 0.5 μM WS-12 stimuli in control condition (top) and including a 10 min staurosporine treatment (bottom) in trigeminal neurons. Black and red arrows on the $[Ca^{2+}]_i$ traces indicate the maximal responses in each condition. ***E***, Bar graph and data points represent the WS-12 ratio response (WS-12 2/WS-12 1) to 0.5 μM WS-12 stimuli, in control condition and with kinase inhibition treatment. Statistical significance was assessed with a two-tailed unpaired Student's *t* test with Welch's correction ($t_{(11)} = 3.226$, $p = 0.0081$; Control, $n = 11$, Sta., $n = 9$). The maximal response (ΔRatio F_{340}/F_{380}) to the first application of WS-12 was 0.180 ± 0.04 ($n = 11$) and 0.249 ± 0.05 ($n = 9$) in both groups, respectively ($t_{(18)} = 1.105$, $p = 0.2837$, unpaired *t* test). Data in the bar graphs are mean ± SE. Statistical significance was assessed with two-tailed unpaired *t* test in all cases: *$p < 0.05$; **$p < 0.01$; ***$p < 0.001$).

our experimental measurements (Fig. 11*D*). The model also predicts that either the shift of TRPM8 $V_{1/2}$ or the increase in g_{max} alone, have a partial but still significant effect (Fig. 11*B–D*).

Interestingly, the simulation of an unphosphorylated S29 TRPM8 condition caused a shift in the mean temperature threshold (Fig. 11*B*), a change also observed when the same neuron is studied before and after kinase inhibition (see Fig. 10*C*). The mean shift in the temperature threshold is larger in the simulation (T. $threshold_{\Delta V1/2\ -50\ mV\ +\ gM8x1.4}$ - T. $threshold_{control}$ = 3.5 ± 0.3°C) than the one observed in cultured neurons (see Fig. 10*C*). However, it has to be considered that, in our model, only TRPM8 has been manipulated, and the experimental situation could include potential effects of kinases inhibition on other ion channels involved in the setting of the CTN thermal threshold.

The spontaneous and cold-evoked firing of corneal cold thermoreceptors is mostly dependent on the functional expression of TRPM8 channels (Parra et al., 2010; Olivares et al., 2015). The electrical activity of these cold-sensitive nerve fibers is critical for maintaining the humidity of the ocular surface by tonically modulating basal tearing and spontaneous blinking under physiological and physiopathological conditions (Parra et al., 2010; Quallo et al., 2015; Piña et al., 2019). To estimate the effect of S29 phosphorylation in TRPM8 regulation in the context of intact nerve endings, we simulated the changes produced in a model tuned to reproduce the behavior of corneal cold-sensitive nerve fibers (Olivares and Orio, 2015; Piña et al., 2019; Rivera et al., 2020). When combined, the increased TRPM8 plasma membrane expression (simulated by an increase in the g_{max}) and the shift of the $V_{1/2}$ toward more negative membrane potentials strongly modified the basal firing, temperature threshold, and maximal cold-evoked response of these cold-sensitive nerve endings (Fig. 12*A*). When applied separately, these maneuvers also showed a partial effect, although the increase in the g_{max} did not induce a significant shift in the temperature threshold (Fig. 12*B–D*). Thus,

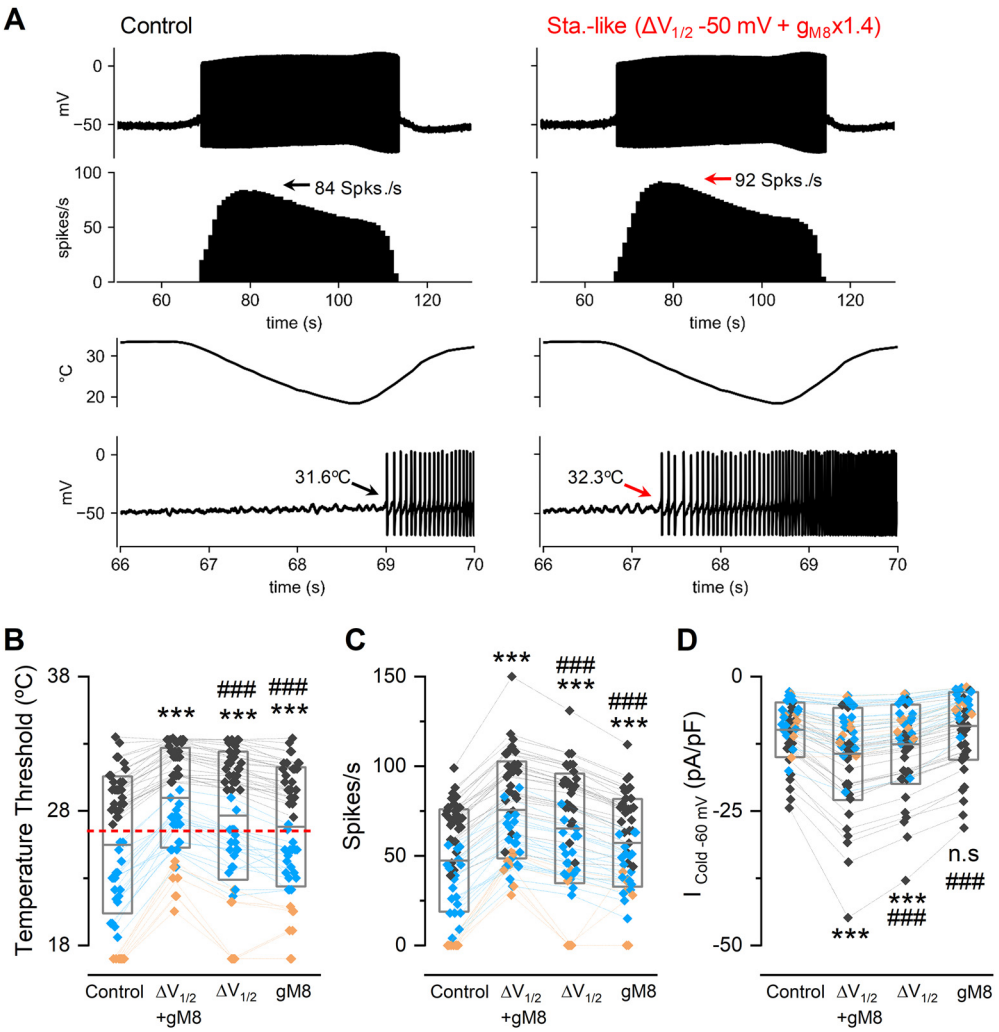

Figure 11. Mathematical model of CTNs firing simulating TRPM8 dephosphorylation. ***A***, Current-clamp simulations (see Materials and Methods) of a CTN with its control parameters (left) and with staurosporine-like TRPM8 conditions ($\Delta V_{1/2}$ −50 mV + g_{M8} x1.4, right) exposed to the same temperature ramps (third row). First row, Membrane potential (in mV). Second row, Firing rate (spikes/s). Bottom row, Zoom of the first action potentials evoked by cold and their temperature thresholds. ***B***, Temperature thresholds for 52 sets of parameters ("individuals"; see Extended Data Figure 11-1) yielding different neuronal behaviors at basal conditions. Black diamonds represent low-threshold CTNs. Blue diamonds represent high-threshold CTNs. Orange diamonds represent neurons that do not respond to the cold pulse (CINs). The control condition refers to the parameters listed in Extended Data Figure 11-1. In the case of individuals that do not respond to a 18°C cold pulse, an arbitrary thermal threshold of 17°C was considered for graphical representation and statistical analysis. Changes in $V_{1/2}$ and g_{max} for TRPM8 ($\Delta V_{1/2}$ −50 mV + g_{M8} x1.4) induce the recruitment of several former CINs (orange diamonds) as cold-sensitive. Dashed red line indicates the previously defined 26.5°C boundary between low- and high-threshold responses (Madrid et al., 2009). ***C***, Firing rate during cooling down to 18°C in the same conditions shown in ***B***. ***D***, Maximum I_{cold} at −60 mV obtained from the model. ***B-D***, Boxes represent the mean (± SD). Symbols represent the individual data. Colors represent the classification of neurons according to their thermal thresholds in control conditions and are maintained throughout the panels. Statistical analysis was performed using repeated ANOVA (temperature threshold: $F_{(3,153)} = 127.80$, $p < 0.0001$; firing rate: $F_{(3,153)} = 194.50$, $p < 0.0001$; I_{cold}: $F_{(3,153)} = 84.74$, $p < 0.0001$), in combination with a Bonferroni's *post hoc* test: ***$p < 0.001$; ns, $p > 0.05$, compared with the control; $^{###}p < 0.001$, compared with staurosporine-like conditions.

these results support the idea that a reduction of the constitutive phosphorylation of TRPM8 may induce potent and physiologically relevant changes in the electrophysiological properties of TRPM8(+) corneal nerve fibers.

In summary, our experimental and modeling results propose a framework for explaining how constitutive serine-phosphorylation acts as a key negative modulator of TRPM8 channel function, mainly through the S29 residue on the distal N-terminus. We show that inhibition of basal kinase activity potentiates TRPM8 function by two complementary mechanisms: (1) a leftward shift of ~50 mV in the voltage-dependent activation, increasing the probability of channel opening at more physiologically relevant membrane potentials; and (2) enhanced functional channel expression at the plasma membrane, both with additive effects on the electrical response of cold thermoreceptors. A graphical representation of our results regarding basal phosphorylation on TRPM8 channel function in primary sensory neurons is shown in Figure 13.

Discussion

The main finding of this study is the demonstration that serine-phosphorylation acts as a key negative modulator of mammalian TRPM8 channel function, regulating cold sensitivity in primary sensory neurons. Specifically, our results suggest that phosphorylation of serine 29 under resting conditions acts as a reversible brake of channel gating and determines the abundance of TRPM8 at the cell surface.

We identified four basally phosphorylated serines within the N-terminus by MS. Remarkably, potentiated responses of TRPM8 channels after kinase inhibition are only mimicked by the single S29A mutation. S26A and S541A+S542A mutants

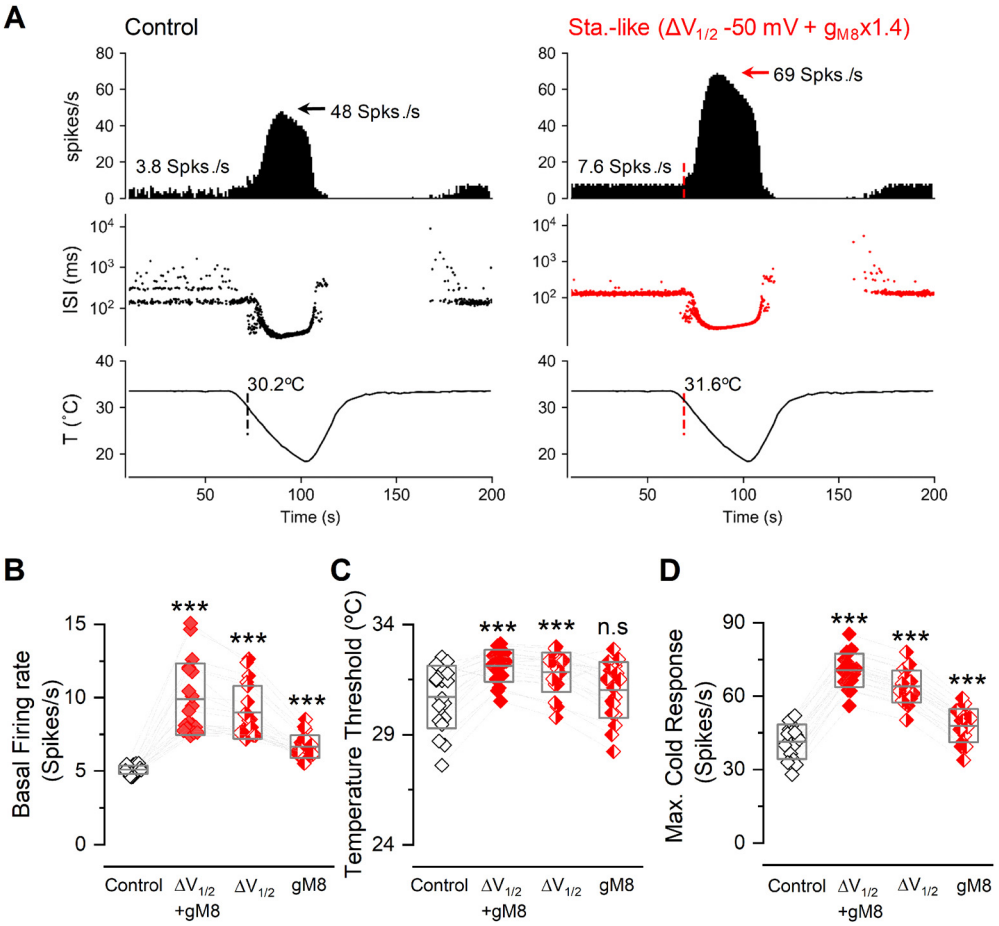

Figure 12. Mathematical model of cold-sensitive nerve endings simulating TRPM8 dephosphorylation. ***A***, Simulated firing activity of a corneal cold thermoreceptor nerve ending model (see Materials and Methods) during a cooling ramp (bottom row), under normal (Control) and simulated dephosphorylated TRPM8 (staurosporine-like) conditions (i.e., $\Delta V_{1/2}$ −50 mV + g_{M8} x1.4 TRPM8). Top row, Average firing rate (spikes/s). Middle row, Interspike intervals (ISI) plots in a log scale. Vertical lines indicate the moment and the temperature value at which the firing rate exceeds the mean + 3 times the SD of the basal firing activity (cold thermal threshold), depicted in top traces. Note the spontaneous firing of action potentials at 33.5°C in both cases. ***B***, Firing rate at 33.5°C for 19 sets of parameters (different cold-sensitive nerve endings; see Extended Data Figure 12-1), with different densities of TRPM8 conductance and $V_{1/2}$. For each model, the normal density of TRPM8 maximal conductance (i.e., gM8 factor = 1.0) is the density that gives a basal firing rate around 5 spikes/s. ***C***, Temperature threshold for cold-evoked activity in the same conditions shown in ***B***. ***D***, Maximum firing rate during the cold pulse for the simulations shown in ***B*** and ***C***. ***B-D***, Boxes represent the mean (± SD). Symbols represent the individual data. Each data point is the average of 10 independent simulations with the same set of parameters. Half-colored red diamonds represent the effect of manipulating only one parameter in each case (g_{max} or $V_{1/2}$), as indicated. Statistical analysis was performed using the one-way ANOVA test (basal firing rate: $F_{(3,54)} = 68.57$, $p < 0.0001$; temperature threshold: $F_{(3,54)} = 23.89$, $p < 0.0001$; maximal cold response: $F_{(3,54)} = 942.7$, $p < 0.0001$), in combination with a Dunnett's *post hoc* test: ns, $p > 0.05$; ***$p < 0.001$, compared with the control.

showed only small alterations in their responses to TRPM8 activators, suggesting that these serine residues do not contribute to the same extent to channel modulation. Corroborating the secondary role of these amino acids in TRPM8 modulation, we previously reported that a different S26 unphosphorylated mutant (S26V), and a chimera where the 507-546 amino acids were replaced by the chicken ortholog sequence that lacks serines 541 and 542, did not exhibit major differences in their responses to cold and menthol compared with the WT channel either (Pertusa et al., 2014, 2018). Considering that functionally important phosphosites are more likely to be conserved across species (Beltrao et al., 2012), it is important to mention that S26 and S29 are well conserved, whereas serines 541 and 542 are absent in several TRPM8 orthologs (see Fig. 1*C*).

Conformational plasticity can facilitate the phosphorylation of specific residues in a protein (Wright and Dyson, 2015). In this regard, S26 and S29 are located in a region predicted as intrinsically disordered (Linding et al., 2003). Recent TRPM8 structures obtained by cryo-electron microscopy lacked resolution of the N-terminus distal part (Diver et al., 2019; Yin et al., 2019), in agreement with a high flexibility of this domain. Moreover, this region acts as an inhibitory domain of TRPM8 function (Pertusa et al., 2014). Truncation of this part of the protein results in a gain-of-function phenotype that could be reproduced by performing 5-10 amino acid deletions or substitutions within this region, or mutating S27 to proline. S27A mutation did not yield channels with augmented responses to cold and menthol, suggesting that introducing a proline at position 27 alters distal TRPM8 N-terminus structure, preventing the negative modulation exerted by this region (Pertusa et al., 2014). Notably, the S27P mutant induces a 50 mV shift in the voltage activation curve of TRPM8 toward more negative membrane potentials (Pertusa et al., 2014), equivalent to the one displayed by the S29A mutation. This result suggests that S29 phosphorylation, probably through the negative charges provided by the phosphate group, is involved in the structural inhibitory role of the distal part of the N-terminus on TRPM8 function. Our new findings suggest that the N-terminal distal domain of TRPM8 can function as a reversible, phosphorylation-dependent brake of TRPM8 activity, modulating the cold sensitivity of CTNs. In

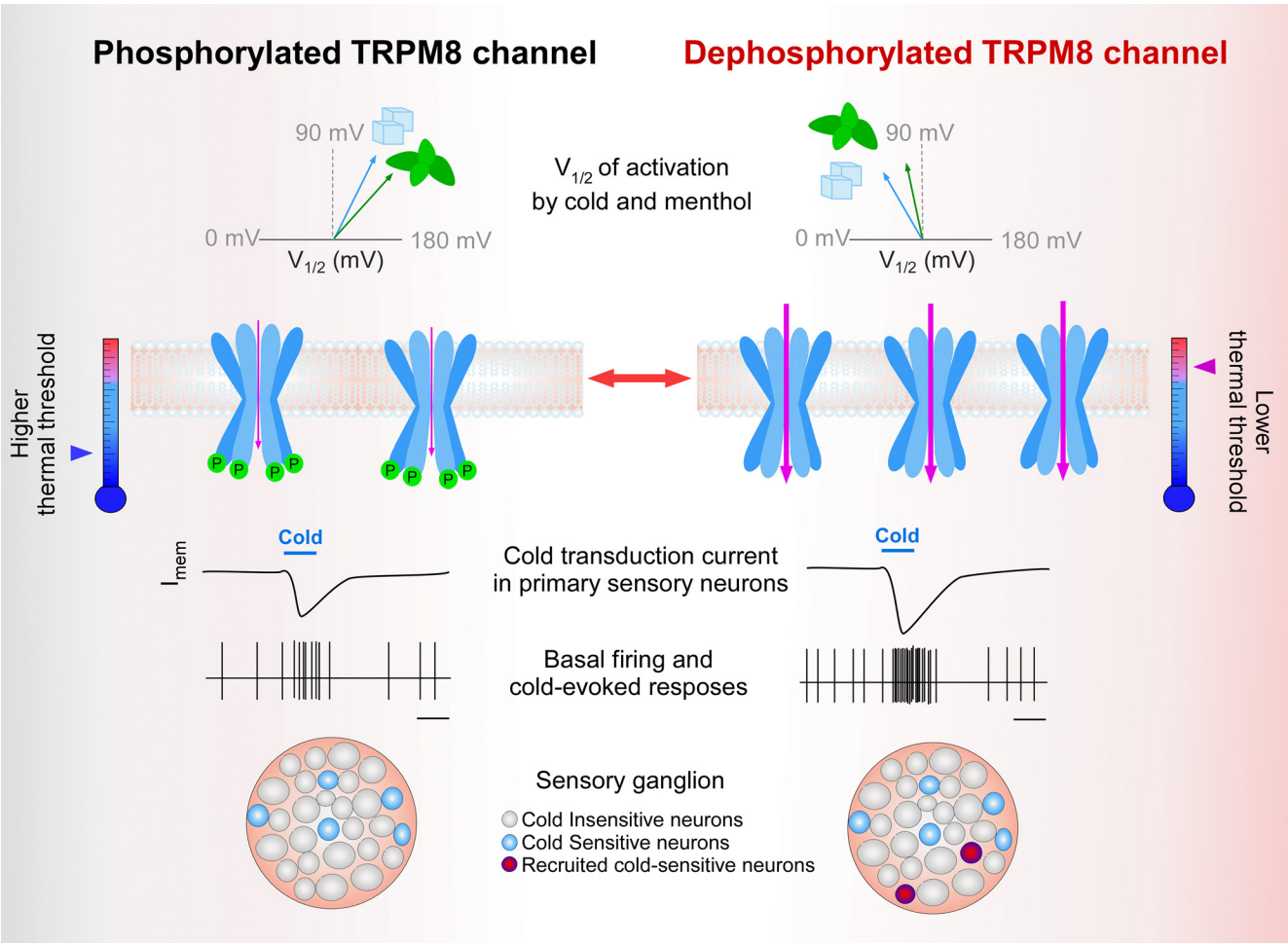

Figure 13. Graphical representation of the effect of basal phosphorylation on TRPM8 channel function. Left column, Schematic representation of $V_{1/2}$ (top row), and membrane availability (second row) and functional properties (lower rows) of phosphorylated TRPM8 channels under basal conditions. Arrow at the thermometer indicates the mean thermal threshold of the cell as the results of this set of parameters. Right column, Potentiated responses to cold and menthol of unphosphorylated TRPM8 channels are because of a shift in the activation $V_{1/2}$ toward more negative membrane potentials and an increase in the number of active channels at the plasma membrane. The number of channels in the scheme at right reflects the expected changes in expression level at the plasma membrane of dephosphorylated TRPM8 channels. Basal kinase activity downregulates TRPM8 function in cold thermoreceptor neurons, suggesting that cold sensing could be fine-tuned by controlling the phosphorylation state of the channel and adjusting the population of CSNs (third to fifth row). Among the basally phosphorylatable amino acids we identified, serine 29 is the most relevant phospho-residue that negatively modulates TRPM8 in resting conditions, acting as a reversible brake on channel function.

addition to this alteration in TRPM8 biophysical properties, S29 phosphorylation also determines TRPM8 expression levels at the plasma membrane, an effect we did not observe in the S27P mutant (Pertusa et al., 2014). This reveals a dual dynamic mechanism by which phosphorylation in the N-terminal distal domain could contribute to TRPM8 regulation.

Although S29A mostly recapitulates the potentiated response observed after kinase activity inhibition, this mutant still exhibits a modest potentiation of the cold-evoked response after treatment with staurosporine, suggesting that phosphorylation of other residues could play some additional, albeit minor, role. In this regard, our immunoprecipitation results showed that threonine residues could also be subject to constitutive phosphorylation. The MS analysis identified some TRPM8 peptides that exhibited variations in mass that were compatible with threonine phosphorylation (data not shown). However, we could not unambiguously determine which residue contains this modification, and further studies are required for their formal identification and to explore their putative contribution to TRPM8 functional modulation.

Constitutive phosphorylation of residues other than S29 can upregulate TRPM8 function. Specifically, the reduction in TRPM8 responses after activation of $G_{\alpha i}$ protein is thought to be because of inhibition of PKA-dependent basal phosphorylation of TRPM8 on residues S9 and T17, implying that phosphorylation of these residues could act as a positive modulator of TRPM8 function in that context (Bavencoffe et al., 2010). In that study, TRPM8 phosphorylation status was assumed, based on the electrophysiological results obtained using single-point mutants, but the direct phosphorylation of TRPM8 by PKA was not established. Tyrosine phosphorylation has also been reported in TRPM8. The authors observed that *src* kinase inhibition produced tachyphylaxis of cold-induced Ca^{2+} transients, suggesting that this PTM could act as a positive modulator of TRPM8 activity, preventing channel desensitization (Manolache et al., 2020). Although we did not identify tyrosine phosphorylated residues or phosphorylation of S9 and T17, this could be because of incomplete coverage of the TRPM8 sequence. Finally, other studies also suggested that PKC-dependent changes in the TRPM8 phosphorylation state result in altered responses to cold and chemical agonists (Premkumar et al., 2005; Iftinca et al., 2020). Therefore, if the phosphorylation of particular residues differently affects TRPM8 function, the existence of diverse phosphorylation

patterns could act as a physiologically relevant mechanism to fine-tune its behavior in specific cellular contexts.

Our study unveils a novel mechanism by which TRPM8 availability at the plasma membrane is regulated. TRPM8 channel expression at the cell surface is the result of dynamic mechanisms promoting exocytosis, endocytosis, and degradation. Membrane proteins are removed from the cell surface by endocytosis and are then either recycled back to the membrane or degraded. Importantly, the rate of these processes is often regulated by kinase activity (Drake et al., 2006; Kennedy and Ehlers, 2006; Jacob et al., 2008). We found that 10 min of incubation in staurosporine was sufficient to observe significant TRPM8 accumulation at the plasma membrane. Thus, we speculate that alteration in the endocytosis and/or recycling rate of TRPM8, rather than synthesis and forward trafficking of the channels from the endoplasmic reticulum, could explain this observation. Further studies are required to fully establish whether basal phosphorylation of TRPM8 could either facilitate their endocytosis or prevent channel recycling.

Molecular mechanisms that govern TRPM8 expression at the cell surface are still poorly understood. Studies using TIRF microscopy revealed that prolonged cold or menthol stimulation increases TRPM8 membrane availability (Toro et al., 2015), and vesicle-associated membrane protein 7 participates in the exocytosis of TRPM8 through atypical secretory vesicles with lysosomal-associated membrane protein 1 and RAB7 molecular identity (Ghosh et al., 2016). Recently, we also described a non-conventional axonal trafficking mechanism involved in delivering TRPM8 channels to the plasma membrane (Cornejo et al., 2020). Our new findings suggest that TRPM8 phosphorylation could be relevant in the dynamic regulation of TRPM8 abundance at the plasma membrane in primary sensory neurons.

We examined the impact of basal phosphorylation on the activity of trigeminal CTNs. We found that staurosporine increased the amplitude of TRPM8-dependent currents and the size of the population of CSNs, suggesting that TRPM8 regulation by basal phosphorylation occurs in native CTNs, and influences their cold-evoked response and thermosensitivity. This is important because TRPM8 activity is known to play a critical role in cold allodynia (Colburn et al., 2007; Knowlton et al., 2013; González et al., 2017). Our computer simulations, using the model of the isolated soma of CSNs, suggest that, under unphosphorylated TRPM8 conditions, additional (i.e., former cold-insensitive) neurons can be recruited to fire during cooling ramps, in strong agreement with our experimental findings, and similar to the changes reported in damage-triggered sensory alterations involving painful cold hypersensitivity (Serra et al., 2009; Yarmolinsky et al., 2016; González et al., 2017; MacDonald et al., 2021). Therefore, one possibility is that the TRPM8 phosphorylation pattern could be altered following nerve injury, contributing to the painful phenotype. In this regard, a gain-of-function R30Q mutation in TRPM8 has been recently identified in a patient affected with trigeminal neuralgia (Gualdani et al., 2021). Because of the close proximity of R30 to the S29 residue, we speculate that the R30Q mutation could either prevent the S29 phosphorylation itself or the effect caused by this PTM, explaining the enhanced responses exhibited by this mutation. Moreover, TRPM8 also controls basal tearing rate (Parra et al., 2010) and blinking frequency (Quallo et al., 2015), and is involved in altered lacrimation and cold hypersensitivity resulting from corneal nerve damage (Piña et al., 2019). Interestingly, our cold corneal thermoreceptor model predicts that both the basal firing and the maximal response to cold of their nerve endings could be strongly increased by TRPM8 dephosphorylation, suggesting a novel approach to regulate the basal tearing rate under pathologic conditions, such as some forms of dry eye disease (Belmonte and Gallar, 2011).

We propose that TRPM8 constitutive phosphorylation contributes to CTNs' net response to cold. Therefore, this form of reversible regulation should be considered when studying pathologic conditions resulting in altered TRPM8 function. Experimental strategies that could take advantage of this regulatory mechanism to palliate TRPM8 dysfunction will require a deeper characterization of how TRPM8 phosphorylation pattern depends on pathophysiological conditions, and which specific kinases and phosphatases participate in maintaining the TRPM8 phosphorylation state.

References

Abe J, Hosokawa H, Sawada Y, Matsumura K, Kobayashi S (2006) Ca^{2+}-dependent PKC activation mediates menthol-induced desensitization of transient receptor potential M8. Neurosci Lett 397:140–144.

Almaraz L, Manenschijn JA, de la Peña E, Viana F (2014) TRPM8. Handb Exp Pharmacol 222:547–579.

Alvarez O, Gonzalez C, Latorre R (2002) Counting channels: a tutorial guide on ion channel fluctuation analysis. Adv Physiol Educ 26:327–341.

Ardito F, Giuliani M, Perrone D, Troiano G, Muzio LL (2017) The crucial role of protein phosphorylation in cell signaling and its use as targeted therapy (Review). Int J Mol Med 40:271–280.

Bavencoffe A, Gkika D, Kondratskyi A, Beck B, Borowiec AS, Bidaux G, Busserolles J, Eschalier A, Shuba Y, Skryma R, Prevarskaya N (2010) The transient receptor potential channel TRPM8 is inhibited via the α2A adrenoreceptor signaling pathway. J Biol Chem 285:9410–9419.

Belmonte C, Gallar J (2011) Cold thermoreceptors, unexpected players in tear production and ocular dryness sensations. Invest Ophthalmol Vis Sci 52:3888–3892.

Beltrao P, Albanèse V, Kenner LR, Swaney DL, Burlingame A, Villén J, Lim WA, Fraser JS, Frydman J, Krogan NJ (2012) Systematic functional prioritization of protein posttranslational modifications. Cell 150:413–425.

Bidaux G, Borowiec AS, Dubois C, Delcourt P, Schulz C, Abeele F, Vanden Lepage G, Desruelles E, Bokhobza A, Dewailly E, Slomianny C, Roudbaraki M, Héliot L, Bonnal JL, Mauroy B, Mariot P, Lemonnier L, Prevarskaya N (2016) Targeting of short TRPM8 isoforms induces 4TM-TRPM8-dependent apoptosis in prostate cancer cells. Oncotarget 7:29063–29080.

Bödding M, Wissenbach U, Flockerzi V (2007) Characterisation of TRPM8 as a pharmacophore receptor. Cell Calcium 42:618–628.

Brauchi S, Orio P, Latorre R (2004) Clues to understanding cold sensation: thermodynamics and electrophysiological analysis of the cold receptor TRPM8. Proc Natl Acad Sci USA 101:15494–15499.

Cerda O, Cáceres M, Park KS, Leiva-Salcedo E, Romero A, Varela D, Trimmer JS, Stutzin A (2015) Casein kinase-mediated phosphorylation of serine 839 is necessary for basolateral localization of the Ca^{2+}-activated non-selective cation channel TRPM4. Pflugers Arch 467:1723–1732.

Colburn RW, Lubin ML, Stone DJ, Wang Y, Lawrence D, D'Andrea MR, Brandt MR, Liu Y, Flores CM, Qin N (2007) Attenuated cold sensitivity in TRPM8 null mice. Neuron 54:379–386.

Cornejo VH, González C, Campos M, Vargas-Saturno L, de los Ángeles Juricic M, Miserey-Lenkei S, Pertusa M, Madrid R, Couve A (2020) Non-conventional axonal organelles control TRPM8 ion channel trafficking and peripheral cold sensing. Cell Rep 30:4505–4517.e5.

de la Peña E, Mälkiä A, Cabedo H, Belmonte C, Viana F (2005) The contribution of TRPM8 channels to cold sensing in mammalian neurones. J Physiol 567:415–426.

De Petrocellis L, Starowicz K, Moriello AS, Vivese M, Orlando P, Di Marzo V (2007) Regulation of transient receptor potential channels of melastatin type 8 (TRPM8): effect of cAMP, cannabinoid CB1 receptors and endovanilloids. Exp Cell Res 313:1911–1920.

Diver MM, Cheng Y, Julius D (2019) Structural insights into TRPM8 inhibition and desensitization. Science 365:1434–1440.

Dragoni I, Guida E, McIntyre P (2006) The cold and menthol receptor TRPM8 contains a functionally important double cysteine motif. J Biol Chem 281:37353–37360.

Drake MT, Shenoy SK, Lefkowitz RJ (2006) Trafficking of G protein-coupled receptors. Circ Res 99:570–582.

Erler I, Al-Ansary DM, Wissenbach U, Wagner TF, Flockerzi V, Niemeyer BA (2006) Trafficking and assembly of the cold-sensitive TRPM8 channel. J Biol Chem 281:38396–38404.

Ghosh D, Pinto S, Danglot L, Vandewauw I, Segal A, Van Ranst N, Benoit M, Janssens A, Vennekens R, Vanden Berghe P, Galli T, Vriens J, Voets T (2016) VAMP7 regulates constitutive membrane incorporation of the cold-activated channel TRPM8. Nat Commun 7:10489.

Gkika D, Lemonnier L, Shapovalov G, Gordienko D, Poux C, Bernardini M, Bokhobza A, Bidaux G, Degerny C, Verreman K, Guarmit B, Benahmed M, de Launoit Y, Bindels RJ, Pla AF, Prevarskaya N (2015) TRP channel-associated factors are a novel protein family that regulates TRPM8 trafficking and activity. J Cell Biol 208:89–107.

González A, Ugarte G, Piña R, Pertusa M, Madrid R (2015) TRP channels in cold transduction. In: TRP channels in sensory transduction, pp 185–207. Cham, Switzerland: Springer International.

González A, Ugarte G, Restrepo C, Herrera G, Piña R, Gómez-Sánchez JA, Pertusa M, Orio P, Madrid R (2017) Role of the excitability brake potassium current IKD in cold allodynia induced by chronic peripheral nerve injury. J Neurosci 37:3109–3126.

Gualdani R, Yuan JH, Effraim PR, Di Stefano G, Truini A, Cruccu G, Dib-Hajj SD, Gailly P, Waxman SG (2021) Trigeminal neuralgia TRPM8 mutation. Neurol Genet 7:e550.

Hines ML, Carnevale NT (1997) The NEURON simulation environment. Neural Comput 9:1179–1209.

Hines ML, Davison AP, Muller E (2009) NEURON and Python. Front Neuroinform 3:1.

Huttlin EL, Jedrychowski MP, Elias JE, Goswami T, Rad R, Beausoleil SA, Villén J, Haas W, Sowa ME, Gygi SP (2010) A tissue-specific atlas of mouse protein phosphorylation and expression. Cell 143:1174–1189.

Iftinca M, Basso L, Flynn R, Kwok C, Roland C, Hassan A, Defaye M, Ramachandran R, Trang T, Altier C (2020) Chronic morphine regulates TRPM8 channels via MOR-PKCβ signaling. Mol Brain 13:61.

Jacob TC, Moss SJ, Jurd R (2008) GABA A receptor trafficking and its role in the dynamic modulation of neuronal inhibition. Nat Rev Neurosci 9:331–343.

Kennedy MJ, Ehlers MD (2006) Organelles and trafficking machinery for postsynaptic plasticity. Annu Rev Neurosci 29:325–362.

Knowlton WM, Palkar R, Lippoldt EK, McCoy DD, Baluch F, Chen J, McKemy DD (2013) A sensory-labeled line for cold: TRPM8-expressing sensory neurons define the cellular basis for cold, cold pain, and cooling-mediated analgesia. J Neurosci 33:2837–2848.

Linding R, Jensen LJ, Diella F, Bork P, Gibson TJ, Russell RB (2003) Protein disorder prediction: implications for structural proteomics. Structure 11:1453–1459.

Linte RM, Ciobanu C, Reid G, Babes A (2007) Desensitization of cold- and menthol-sensitive rat dorsal root ganglion neurones by inflammatory mediators. Exp Brain Res 178:89–98.

Liu B, Qin F (2005) Functional control of cold- and menthol-sensitive TRPM8 ion channels by phosphatidylinositol 4,5-bisphosphate. J Neurosci 25:1674–1681.

MacDonald DI, Luiz AP, Iseppon F, Millet Q, Emery EC, Wood JN (2021) Silent cold-sensing neurons contribute to cold allodynia in neuropathic pain. Brain 144:1711–1726.

Madrid R, de la Pena E, Donovan-Rodriguez T, Belmonte C, Viana F (2009) Variable threshold of trigeminal cold-thermosensitive neurons is determined by a balance between TRPM8 and Kv1 potassium channels. J Neurosci 29:3120–3131.

Madrid R, Pertusa M (2014) Intimacies and physiological role of the polymodal cold-sensitive ion channel TRPM8. Curr Top Membr 74:293–324.

Mälkiä A, Madrid R, Meseguer V, De La Peña E, Valero M, Belmonte C, Viana F (2007) Bidirectional shifts of TRPM8 channel gating by temperature and chemical agents modulate the cold sensitivity of mammalian thermoreceptors. J Physiol 581:155–174.

Manolache A, Selescu T, Maier GL, Mentel M, Ionescu AE, Neacsu C, Babes A, Szedlacsek SE (2020) Regulation of TRPM8 channel activity by Src-mediated tyrosine phosphorylation. J Cell Physiol 235:5192–5203.

McCoy DD, Knowlton WM, McKemy DD (2011) Scraping through the ice: uncovering the role of TRPM8 in cold transduction. Am J Physiol Regul Integr Comp Physiol 300:R1278–R1287.

McKemy DD (2013) The molecular and cellular basis of cold sensation. ACS Chem Neurosci 4:238–247.

McKemy DD (2018) Molecular basis of peripheral innocuous cold sensitivity. In: Handbook of clinical neurology, pp 57–67. Elsevier, Amsterdam.

McKemy DD, Neuhausser WM, Julius D (2002) Identification of a cold receptor reveals a general role for TRP channels in thermosensation. Nature 416:52–58.

Morenilla-Palao C, Pertusa M, Meseguer V, Cabedo H, Viana F (2009) Lipid raft segregation modulates TRPM8 channel activity. J Biol Chem 284:9215–9224.

Nilius B, Mahieu F, Prenen J, Janssens A, Owsianik G, Vennekens R, Voets T (2006) The Ca^{2+}-activated cation channel TRPM4 is regulated by phosphatidylinositol 4,5-biphosphate. EMBO J 25:467–478.

Olivares E, Orio P (2015) Mathematical modeling of TRPM8 and the cold thermoreceptors. In: TRP channels in sensory transduction, pp 209–223. Cham, Switzerland: Springer International.

Olivares E, Salgado S, Maidana JP, Herrera G, Campos M, Madrid R, Orio P (2015) TRPM8-dependent dynamic response in a mathematical model of cold thermoreceptor. PLoS One 10:e0139314.

Pabbidi MR, Premkumar LS (2017) Role of transient receptor potential channels Trpv1 and Trpm8 in diabetic peripheral neuropathy. J Diabetes Treat 2017:4. [PMC]

Paricio-Montesinos R, Schwaller F, Udhayachandran A, Rau F, Walcher J, Evangelista R, Vriens J, Voets T, Poulet JF, Lewin GR (2020) The sensory coding of warm perception. Neuron 106:830–841.e3.

Parra A, Madrid R, Echevarria D, del Olmo S, Morenilla-Palao C, Acosta MC, Gallar J, Dhaka A, Viana F, Belmonte C (2010) Ocular surface wetness is regulated by TRPM8-dependent cold thermoreceptors of the cornea. Nat Med 16:1396–1399.

Peier AM, Moqrich A, Hergarden AC, Reeve AJ, Andersson DA, Story GM, Earley TJ, Dragoni I, McIntyre P, Bevan S, Patapoutian A (2002) A TRP channel that senses cold stimuli and menthol. Cell 108:705–715.

Pérez de Vega MJ, Gómez-Monterrey I, Ferrer-Montiel A, González-Muñiz R (2016) Transient receptor potential melastatin 8 channel (TRPM8) modulation: cool entryway for treating pain and cancer. J Med Chem 59:10006–10029.

Pertusa M, González A, Hardy P, Madrid R, Viana F (2014) Bidirectional modulation of thermal and chemical sensitivity of TRPM8 channels by the initial region of the N-terminal domain. J Biol Chem 289:21828–21843.

Pertusa M, Madrid R (2015) Modulation of TRP channels by N-glycosylation and phosphorylation. In: TRP channels in sensory transduction, pp 73–96. Cham, Switzerland: Springer International.

Pertusa M, Madrid R, Morenilla-Palao C, Belmonte C, Viana F (2012) N-glycosylation of TRPM8 ion channels modulates temperature sensitivity of cold thermoreceptor neurons. J Biol Chem 287:18218–18229.

Pertusa M, Rivera B, González A, Ugarte G, Madrid R (2018) Critical role of the pore domain in the cold response of TRPM8 channels identified by ortholog functional comparison. J Biol Chem 293:12454–12471.

Piña R, Ugarte G, Campos M, Íñigo-Portugués A, Olivares E, Orio P, Belmonte C, Bacigalupo J, Madrid R (2019) Role of TRPM8 channels in altered cold sensitivity of corneal primary sensory neurons induced by axonal damage. J Neurosci 39:8177–8192.

Premkumar LS, Raisinghani M, Pingle SC, Long C, Pimentel F (2005) Downregulation of transient receptor potential melastatin 8 by protein kinase C-mediated dephosphorylation. J Neurosci 25:11322–11329.

Quallo T, Vastani N, Horridge E, Gentry C, Parra A, Moss S, Viana F, Belmonte C, Andersson DA, Bevan S (2015) TRPM8 is a neuronal osmosensor that regulates eye blinking in mice. Nat Commun 6:7150–7112.

Rivera B, Campos M, Orio P, Madrid R, Pertusa M (2020) Negative modulation of TRPM8 channel function by protein kinase C in trigeminal cold thermoreceptor neurons. Int J Mol Sci 21:4420.

Rohacs T, Lopes CM, Michailidis I, Logothetis DE (2005) PI(4,5)P2 regulates the activation and desensitization of TRPM8 channels through the TRP domain. Nat Neurosci 8:626–634.

Sabnis AS, Shadid M, Yost GS, Reilly CA (2008) Human lung epithelial cells express a functional cold-sensing TRPM8 variant. Am J Respir Cell Mol Biol 39:466–474.

Sarria I, Gu J (2010) Menthol response and adaptation in nociceptive-like and nonnociceptive-like neurons: role of protein kinases. Mol Pain 6:47.

Serra J, Solà R, Quiles C, Casanova-Molla J, Pascual V, Bostock H, Valls-Solé J (2009) C-nociceptors sensitized to cold in a patient with small-fiber neuropathy and cold allodynia. Pain 147:46–53.

Sievers F, Wilm A, Dineen D, Gibson TJ, Karplus K, Li W, Lopez R, McWilliam H, Remmert M, Soding J, Thompson JD, Higgins DG (2011) Fast, scalable generation of high-quality protein multiple sequence alignments using Clustal Omega. Mol Syst Biol 7:539.

Tang Z, Kim A, Masuch T, Park K, Weng HJ, Wetzel C, Dong X (2013) Pirt functions as an endogenous regulator of TRPM8. Nat Commun 4:2179.

Toro CA, Eger S, Veliz L, Sotelo-Hitschfeld P, Cabezas D, Castro MA, Zimmermann K, Brauchi S (2015) Agonist-dependent modulation of cell surface expression of the cold receptor TRPM8. J Neurosci 35:571–582.

Viana F, Voets T (2019) Heat pain and cold pain. Oxford Handb Neurobiol Pain 1–25.

Voets T, Droogmans G, Wissenbach U, Janssens A, Flockerzi V, Nilius B (2004) The principle of temperature-dependent gating in cold- and heat-sensitive TRP channels. Nature 430:748–754.

Vriens J, Nilius B, Voets T (2014) Peripheral thermosensation in mammals. Nat Rev Neurosci 15:573–589.

Waterhouse AM, Procter JB, Martin DM, Clamp M, Barton GJ (2009) Jalview version 2: a multiple sequence alignment editor and analysis workbench. Bioinformatics 25:1189–1191.

Wright PE, Dyson HJ (2015) Intrinsically disordered proteins in cellular signaling and regulation HHS public access. Nat Rev Mol Cell Biol 16:18–29.

Yarmolinsky DA, Peng Y, Pogorzala LA, Rutlin M, Hoon MA, Zuker CS (2016) Coding and plasticity in the mammalian thermosensory system. Neuron 92:1079–1092.

Yin Y, Wu M, Zubcevic L, Borschel WF, Lander GC, Lee SY (2018) Structure of the cold- and menthol-sensing ion channel TRPM8. Science 359:237–241.

Yin Y, Le SC, Hsu AL, Borgnia MJ, Yang H, Lee SY (2019) Structural basis of cooling agent and lipid sensing by the cold-activated TRPM8 channel. Science 363:eaav9334.

Yudin Y, Lukacs V, Cao C, Rohacs T (2011) Decrease in phosphatidylinositol 4,5-bisphosphate levels mediates desensitization of the cold sensor TRPM8 channels. J Physiol 589:6007–6027.

Zhang X, Mak S, Li L, Parra A, Denlinger B, Belmonte C, McNaughton PA (2012) Direct inhibition of the cold-activated TRPM8 ion channel by Gαq. Nat Cell Biol 14:851–858.